

ATTI DEI DIRETTORI DELLE SEZIONI DI RICERCA SCIENTIFICA O TECNOLOGICA, DELLE  
STRUTTURE TECNICHE DI SERVIZIO E DEI DIRIGENTI

**Atto n. GEO 452 ADW del 27/06/2025**

---

**Oggetto:** Pubblicazione in open access dell'articolo scientifico al titolo: "Discovery of cenozoic magmatic ridges and tectonics off Northern Victoria land provides new insights into the geodynamics of the Antarctic margin", sulla rivista "Scientific Reports". Importo complessivo € 2.445,00, IVA esclusa. Oneri di sicurezza interferenziale non soggetti a ribasso d'asta: € 0,00. Affidamento diretto, ai sensi dell'art. 50, comma 1, lettera b), del D.Lgs. n. 36/2023 e s.m.i., alla società Springer Nature Customer Service Center GmbH, di Heidelberg (Germania), VAT Number DE209719094. CIG n. B764FE2BA5, CUP n. B47I18075860006.

**IL DIRETTORE DELLA SEZIONE DI RICERCA SCIENTIFICA GEOFISICA**

**Premesso** che il dott. Dario Civile ha richiesto (Allegato n. 1), di procedere con l'acquisto del servizio di pubblicazione, in open access, dell'articolo scientifico al titolo: "Discovery of cenozoic magmatic ridges and tectonics off Northern Victoria land provides new insights into the geodynamics of the Antarctic margin", sulla rivista "Scientific Reports", (RDF s.n.);

**tenuto conto** del prestigio dell'editore Springer Nature e della diffusione delle sue pubblicazioni;

**ricevuta** e ritenuta congrua, la fattura n. 2936498027 di data 16/06/2025, inviata dalla società Springer Nature Customer Service Center GmbH, di Heidelberg (Germania), contenente il corrispettivo per il servizio richiesto, al costo complessivo di € 2.445,00, IVA esclusa (Allegato n. 2);

**preso atto** che la spesa massima stimata per il servizio risulta inferiore alla soglia di € 5.000,00;

**tenuto conto** inoltre delle disposizioni contenute nella c.d. Legge di Stabilità 2016 (L. 28/12/2015, n. 208), modificata con la c.d. Legge di Stabilità 2019, laddove è possibile effettuare acquisti di beni e servizi di valore inferiore ad € 5.000,00 (IVA esclusa) al di fuori del MePA Consip;

**considerato** l'art. 50, comma 1, lettera b), del D.Lgs. n. 36/2023 e s.m.i. (di seguito "Codice"), laddove si dispone che le stazioni appaltanti possano procedere, per importi inferiori a € 140.000,00, ad affidamenti diretti anche senza previa consultazione di più operatori economici;

**ritenuto** applicabile, nella fattispecie, quanto previsto dall'art. 49, comma 6, del Codice, laddove si consente di derogare al principio di rotazione per affidamenti diretti di importo inferiore ad € 5.000,00, IVA esclusa;

<b>verificato</b>	infine che risultano applicabili le disposizioni di cui all'art. 10, comma 3, del D.Lgs. 25/11/2016, n. 218 (Semplificazione delle attività degli Enti Pubblici di ricerca ai sensi dell'art. 13 della L. 7/8/2015, n. 124), in quanto il servizio in oggetto è funzionalmente collegata e destinata ad attività di ricerca, non sussistendo quindi l'obbligo di ricorso al mercato elettronico della Pubblica Amministrazione (MePA);
<b>visto</b>	l'articolo 26, comma 3 bis del D.Lgs. 9 aprile 2008, n. 81, il servizio di cui trattasi non comporta rischi da interferenza, per cui non è stato redatto il DUVRI;
<b>visto</b>	l'art. 53 comma 4 del Codice laddove si prevede che in casi debitamente motivati è facoltà della stazione appaltante non richiedere la garanzia definitiva per l'esecuzione dei contratti;
<b>considerato</b>	il modesto importo dell'affidamento;
<b>visti</b>	gli articoli 17 e 53 del Codice; gli articoli da 1 a 11 del Codice; l'articolo 15 del Codice, l'Allegato I.2 del Codice e l'articolo 6 della L. 241/1990 e s.m.i.; l'articolo 16 del Codice, relativo all'individuazione e gestione dei conflitti di interesse nelle procedure di affidamento di contratti pubblici; il Patto d'integrità approvato con determinazione del Direttore Generale n. 230 ADW del 12/05/2023;
<b>dato atto</b>	che, ai sensi di quanto disposto dall'art. 15 del D.Lgs. n. 36/2023 e s.m.i., il sottoscritto è il Responsabile Unico del Progetto (RUP) della procedura di cui trattasi;
<b>preso atto</b>	che non ricorrono nel caso di specie motivi di incompatibilità o di conflitto di interesse, nei confronti dello scrivente, ai sensi della vigente normativa in materia di contrasto alla corruzione;
<b>ritenuto</b>	di nominare la sig.ra Simona Cassaro, collaboratore amministrativo dell'Ufficio Centralizzato per gli Acquisti (UCA), responsabile dell'istruttoria della procedura di cui trattasi;
<b>visto</b>	il vigente Regolamento di Amministrazione Contabilità e Finanza dell'OGS;
<b>visto</b>	il Regolamento interno per la definizione delle procedure di acquisto di lavori, servizi e forniture, approvato in data 27/03/2023;
<b>vista</b>	la determinazione della Direttrice Generale n. 112 ADW dd. 05/03/2025 avente ad oggetto: "Delega temporanea in materia di contratti pubblici di lavori, servizi e forniture ai Direttori delle Sezioni e dei Centri di ricerca e delle Strutture Tecniche e ai Dirigenti Amministrativi.";
<b>richiamata</b>	la deliberazione del CdA n. 12 ADW adottata nella seduta del 31.01.2025 avente ad oggetto: "Procedura di valutazione comparativa per l'individuazione del Direttore della Sezione di Geofisica: nomina del Direttore." con la quale si è disposto la nomina a Direttore della Sezione di Ricerca Scientifica Geofisica, del dott. Fausto Ferraccioli con decorrenza 15.02.2025 e termine massimo 14.02.2029;
<b>pertanto</b>	sulla base delle premesse di cui sopra,

## DETERMINA

1. di procedere, per i motivi esposti in premessa, all'affidamento diretto alla società Springer Nature Customer Service Center GmbH, di Heidelberg (Germania), VAT Number DE209719094, del servizio di pubblicazione in open access dell'articolo scientifico al titolo: "Discovery of cenozoic magmatic

ridges and tectonics off Northern Victoria land provides new insights into the geodynamics of the Antarctic margin”, sulla rivista “Scientific Reports”, ai sensi dell’art. 50, comma 1, lettera b), del Codice, al prezzo complessivo di € 2.445,00, IVA esclusa;

2. per le ragioni sopra descritte e per quanto previsto dall’art. 53, comma 4, del Codice, di non richiedere all'affidatario la prestazione della garanzia definitiva;
3. di autorizzare la stipula del contratto mediante scambio di corrispondenza;
4. di dare atto che per la spesa complessiva pari ad € 2.982,90 IVA compresa, è stata effettuata la registrazione anticipata su U.O. GEO n. ID DG 46025, n. registrazione 66/2025, CODICE PROGETTO FARNETO\_comm.5154\_art.222\_n23 FARNETO(c.5154\_a.222\_n23), CUP n. B47I18075860006;
5. di dare atto che, ai sensi di quanto disposto dall’art. 15 del Codice, la Responsabile Unica del Progetto in oggetto è la sottoscritta mentre la sig.ra Simona Cassaro funge da Responsabile dell’Istruttoria;
6. di pubblicare il presente provvedimento sul profilo del committente nella Sezione Amministrazione Trasparente/ Bandi di gara e contratti e di trasmettere il relativo avviso di aggiudicazione alla Banca Dati Nazionale dei Contratti Pubblici mediante la piattaforma di approvvigionamento digitale.

IL DIRETTORE  
Fausto Ferraccioli

# Elenco firmatari

ATTO SOTTOSCRITTO DIGITALMENTE AI SENSI DEL D.P.R. 445/2000 E DEL D.LGS. 82/2005 E SUCCESSIVE MODIFICHE E INTEGRAZIONI

Questo documento è stato firmato da:

NOME: FERRACCIOLI FAUSTO

CODICE FISCALE: FRRFST70A29D969K

DATA FIRMA: 27/06/2025 11:55:26

IMPRONTA: 6CDF783466D70F90DE39D93BCAD1BD37176741258196CB407834E51099CFAC2B  
176741258196CB407834E51099CFAC2B667E24426D855AE31924D3E062538642  
667E24426D855AE31924D3E062538642968A90276972CAFCE0FE084244147350  
968A90276972CAFCE0FE0842441473506A346DF3AD294D1E2A9EDDEC8F3D2A41

### MODULO RICHIESTA FORNITURA IN ECONOMIA

LE RICHIESTE SARANNO NUMERATE A CURA DELL' GRUPPO RICHIEDENTE

STRUTTURA <b>GEO</b> DATA <b>23 /06 /2025</b> RICHIESTA N. <b>/25</b>									RISERVATO ALL'UPA O AL G.S.		
N° PROG.	INV.	CO NS.	DESCRIZIONE	COMMESSA	UNITA' DI MISURA	Q.TA'	IMPORTO	AL. IVA	PREZZO	CONSIP NO Esaurito Prezzo	
1			Pagamento Articolo su SCIENTIFIC REPORTS di Civile et al. (Sezione GEO)	Farneto 5154/222_n23	euro	1	2445	22	2982,9		
NOTE: _____ _____ _____  IL RICHIEDENTE RESP. COMMESSA   VOCE DI SPESA AMMESSA A RENDICONTAZIONE SI NO X									<b>DITTE INTERPELLATE</b>		<b>TOTALE IVA COMPR.</b>
									1 _____		<u>DITTA AFFIDATARIA</u>  <b>SPRINGER NATURE</b>
									2 _____		
									3 _____		
									4 _____		
									5 _____		
<b>RICHIESTA DI RIMBORSO MEDIANTE SERVIZIO INTERNO DI CASSA</b> <input type="checkbox"/> spese per piccole riparazioni, manutenzioni di mobili e locali <input type="checkbox"/> minute spese d'ufficio <input type="checkbox"/> spese di vettura <input type="checkbox"/> spese postali <input type="checkbox"/> spese per giornali, pubblicazioni, periodici e simili  FIRMA PER AVVENUTO RIMBORSO _____									<b>FIRMA PER ACQUISTO TRAMITE SERVIZIO INTERNO DI CASSA</b> <input type="checkbox"/> IL DIRETTORE GENERALE <input type="checkbox"/> IL DIR. DI DIP. O STR. TECN. DI SERV.  <input type="checkbox"/> IL DIRIGENTE AMM.VO		
<b>IDDG</b> _____ <b>nr. Registrazione</b> _____ <b>FIRMA</b> _____ <b>DATA</b> _____				<b>AUTORIZZAZIONE ALL'ACQUISTO</b>  NOTE RELATIVE ALL'AUTORIZZAZIONE DATA _____							
<b>DATA</b> _____ <b>REGISTRAZIONE UFFICIO RAGIONERIA</b> _____			<b>ORDINE EVASO</b> <input type="checkbox"/>		<input type="checkbox"/> IL DIRETTORE GENERALE <input type="checkbox"/> IL DIR. DIP. O DI STR. TECN. SERV. <input type="checkbox"/> IL DIRIGENTE AMM.VO						



## OPEN Discovery of cenozoic magmatic ridges and tectonics off Northern Victoria land provides new insights into the geodynamics of the Antarctic margin

Dario Civile<sup>1,4</sup>✉, Laura Crispini<sup>2,4</sup>, Antonia Ruppel<sup>3</sup>, Giulia Matilde Ferrante<sup>1</sup>, Danilo Morelli<sup>2</sup>, Daniela Accettella<sup>1</sup>, Flavio Accaino<sup>1</sup>, Michele Locatelli<sup>2</sup>, Valentina Volpi<sup>1</sup>, Martina Busetti<sup>1</sup>, Egidio Armadillo<sup>2</sup> & Andreas Läufer<sup>3</sup>

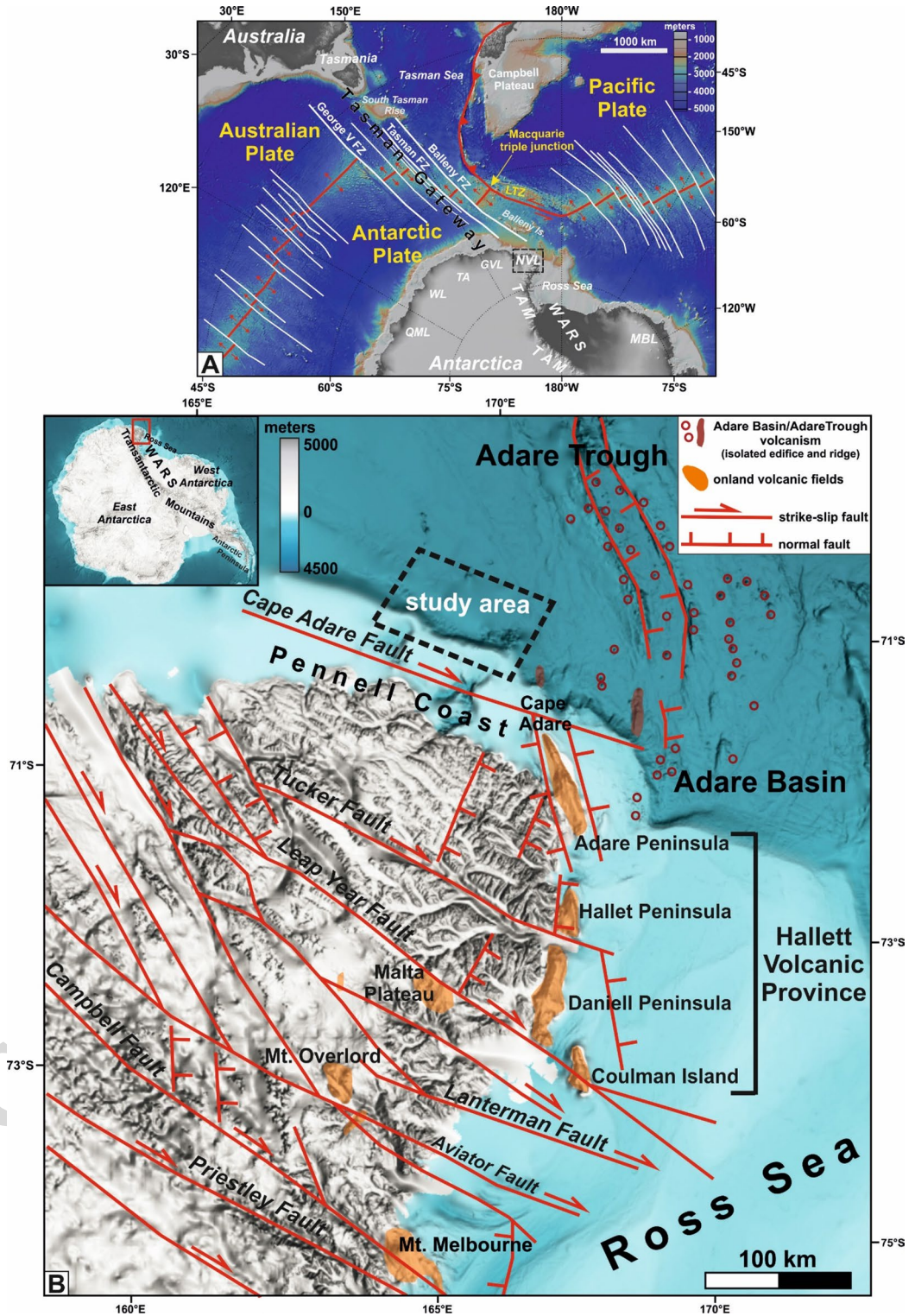
The remote Pacific side of northern Victoria Land (NVL) lies at the boundary between East and West Antarctica and represents the area where the final continental breakup between the Antarctic and Australian conjugate margins occurred, leading to the opening of the Tasman Gateway since the Eocene-Oligocene boundary. Understanding the tectonic evolution of this area is crucial for the geodynamics of the Australian-Antarctic separation and the formation of the independent Antarctic plate in the Late Mesozoic-Cenozoic. This study, based on new multibeam data and multichannel seismic profiles combined with aeromagnetic data, presents an updated picture of the structural architecture of the NVL offshore area. The main novelties of this picture include the discovery of two large active submarine magmatic ridges in the southern sector and an isolated rifted crustal block in the north. The tectonic interpretation supports a NW-oriented, intraplate right-lateral megashear zone with associated magmatism that was active in the Pliocene-Quaternary and was accompanied by thinning of the continental crust. This deformation zone likely represents the intraplate continuation of the Balleny Fracture Zone off NVL and developed along the previous transform plate boundary between the Antarctic and Australian margins, characterized by left-lateral kinematics in the late Eocene-early Oligocene.

**Keywords** Northern Victoria land, Antarctica-Australia separation, Active submarine volcanic ridges, Morpho-bathymetric data, Multichannel seismic profiles, Aeromagnetic data

The Pacific coast of northern Victoria Land (NVL), at the termination of the Transantarctic Mountains along the northwestern end of the Ross Sea, is a remote, underexplored area that is covered by sea ice most of the year (Fig. 1). It lies at the boundary between the East Antarctic craton and the younger, hot and thin lithosphere of the West Antarctic Rift System (WARS)<sup>1,2</sup> (Fig. 1). The WARS is characterized by late Meso- to Cenozoic extension, Cenozoic alkaline magmatism and a strongly uplifted western rift shoulder forming the Transantarctic Mountains, and a less pronounced uplift of its eastern shoulder in Marie Byrd Land (MBL in Fig. 1A) (e.g. Refs<sup>3-8</sup>). Magmatism along the western margin of the WARS occurs in NVL, where it is divided into the Hallett (Fig. 1), Melbourne and Erebus volcanic provinces (the Cenozoic McMurdo Volcanic Group), and in the northwestern Ross Sea region (e.g. Ref<sup>9</sup>).

New offshore geophysical data, consisting of multibeam morpho-bathymetric data, multichannel reflection seismic (MCS) profiles and marine magnetic data, were acquired in February 2023 and 2024 (38th -39th Italian Antarctic Expeditions) along the Pacific coast of the NVL (i.e. Pennell Coast) (Fig. 1) as part of the Italian PNRA (National Antarctic Research Program) BOOST project (Bridging Onshore-Offshore Structures at the Pacific Coast of northern Victoria Land, Antarctica: an integrated approach) on board the OGS R/V “Laura Bassi”. This

<sup>1</sup>National Institute of Oceanography and Applied Geophysics – OGS, Borgo Grotta Gigante, 42/c, Sgonico (Trieste) 34010, Italy. <sup>2</sup>Department of Earth, Environmental and Life Sciences, University of Genova, Genova 16132, Italy. <sup>3</sup>Federal Institute for Geosciences and Natural Resources (BGR), Stilleweg 2, 30655 Hannover, Germany. <sup>4</sup>Dario Civile and Laura Crispini contributed equally to this work. ✉email: dcivile@ogs.it



dataset is combined with vintage aeromagnetic data acquired from the offshore region of NVL (GANOVEX IX campaign 2005–2006) and the multichannel seismic line BGR80-100.

The location of the study area is crucial for understanding the interaction between the tectonic evolution of the WARS and the rift-to-drift transition between NVL and Tasmania during the final continental breakup between the Antarctic and Australian conjugate margins (Fig. 1). This process began at the Eocene-Oligocene boundary (~35–32 Ma) and led to the opening of the deep-water Tasman Gateway<sup>10,11</sup>. This event, together with the opening of the Drake Passage between South America and the Antarctic Peninsula, led to the formation of the Antarctic Circumpolar Current (ACC) around 30 Ma (e.g. Ref<sup>12</sup>). The ACC thermally isolated Antarctica and caused its progressive cooling with the onset of permanent glaciation (e.g. Refs<sup>13,14</sup>). Continental breakup between Australia and Antarctica began in the Cretaceous, followed by a west to east seafloor spreading and associated with the development of a dense array of fracture zones such as the Tasman and Balleny fracture

◀ **Fig. 1.** Geodynamic and tectonic map of the Tasman Gateway and northern Victoria Land. **(A)** Morpho-bathymetric map of the seafloor around the Macquarie Triple Junction, which marks the point where the Australian Plate, Pacific Plate and Antarctic Plate interact. The red lines are the plate boundaries between the Australian, Antarctic and Pacific plates; the white lines are the fracture zones that offset the segments of the mid-ocean ridge. In particular, the major dextral NW-SE Balleny, Tasman and George V fracture zones between the Australian and Antarctic plates are highlighted. The black dashed rectangle indicates the location of northern Victoria Land (NVL). The DEM was made using GMRT, version 4.3.0 ([www.gmrt.org](http://www.gmrt.org)), and the software GeoMapApp, Version 3.7.4 ([www.geomapapp.org](http://www.geomapapp.org); CC by Ryan et al.<sup>22</sup>). Abbreviations: GVL, George V Land; LTZ, leaky transform zone; MBL, Marie Byrd Land; QML, Queen Mary Land; TA, Terre Adélie; TAM, Transantarctic Mountains; WL, Wilkes Land. **(B)** Tectonic sketch map of NVL and its offshore area, which includes the Adare Basin and the Adare Trough (modified and redrawn after<sup>3,6,23</sup>). The location of the main Neogene onshore volcanic fields (orange zones) of NVL (modified after Smellie and Rocchi<sup>9</sup>) and volcanism in the Adare Basin and Adare Trough (red circles and bodies) (modified after Granot et al.<sup>6</sup>) is also indicated. The volcanic fields forming the Hallet Volcanic Province are indicated. These features are superposed onto the IBSCO (International Bathymetric Chart of the Southern Ocean<sup>24</sup>) morpho-bathymetry and topography of NVL. The black dashed rectangle is the location of the area investigated by the BOOST Project. Inset: Location of Figure B on the Antarctic continent. It is located in the northernmost part of the Transantarctic Mountains, which separate West and East Antarctica.

zones and the formation of the Adare Trough as a failed rift arm of a rift-rift-rift triple junction between ~43 and 26 Ma<sup>4,15,16</sup> (Fig. 1). Several regional-scale geodynamic models proposed that the continuation of these fracture zones through the continental crust of NVL to the Ross Sea is represented by NW-SE striking, Cenozoic, intraplate dextral strike-slip fault systems interacting with N-S normal faults<sup>3,17–21</sup> (Fig. 1).

The main objectives of this study are to document and characterize the significant Cenozoic submarine magmatism along the Pacific coast of NVL, provide a detailed analysis of the structural architecture of its offshore region, and develop a geodynamic model to enhance the understanding of the tectonic evolution of this crucial sector of the Antarctic Plate.

## Results

### Morpho-bathymetric features

As illustrated in Fig. 2, multibeam mapping of the seafloor delineates the primary morpho-bathymetric elements of the study area. The seafloor morphology was also analyzed using eight bathymetric profiles (Fig. 2) and 3D views (Fig. 3).

The study area is defined by a wide continental shelf that extends for about 70 km to the south and narrows to about 50 km to the north, with depths between 180 and 400 m below sea level (bsl) (Fig. 2). The shelf morphology is relatively flat, with a maximum slope of ~2°. At both ends of the continental shelf there are two U-shaped, approximately ENE-WSW oriented glacial troughs (already identified by<sup>25</sup>) (Figs. 2 and 3a). These troughs exhibit varying depths, with the southern trough measuring between 750 and 500 mbsl and the northern trough between 1250 and 550 mbsl (bathymetric profiles 1 and 2). The northern trough is notably asymmetric, with a steeper southern flank (up to 30°); the southern steep flank of the southern trough shows an abrupt change in orientation from WNE-WSW to NNE-SSW (Fig. 2). The bottom of both troughs shows parallel, mega-scale lineations (MGPL in Fig. 2) (e.g. Refs<sup>26,27</sup>), which indicate the ice flow direction in the past towards NE.

The continental slope displays sharp changes, characterized by pronounced variations in orientation (Figs. 2 and 3A and B). The northern sector has a N130° orientation, with slopes between 10°–12° and a prominent outward-bulging at the end of the cross-shelf glacial trough, which is incised by a gully network. The central sector has a N110°–115° orientation and slopes up to 18° with a less pronounced outward bulging at the southern glacial trough, which is incised by scattered gullies (Fig. 2 and bathymetric profiles 1 and 2). These sectors are separated by an indentation at the shelf-break (Figs. 2 and 3A), which shows a right-lateral displacement. The two outward-bulging features are trough mouth fans (TMFs) adjacent to the troughs and indicate sediment processes related to shelf propagation in front of ice streams (e.g. Refs<sup>28,29</sup>). In the southernmost sector of the study area, the continental slope has a N-S trend and a maximum inclination of 10°.

On the continental slope and on the inner continental rise, between the two TMFs, channel-levee systems develop orthogonally to the slope, converging into a single channel with a depth exceeding 100 m (CH in Figs. 2 and 3B,C). This channel marks the northern boundary of a large sedimentary wedge likely composed of turbiditic and hemipelagic sediments (Fig. 3A,B). The most significant systems of channel-levee are located at the shelf-break indentation zone. Here, the channels converge seaward and form a single well-carved, roughly N-S oriented channel (CH in Figs. 2 and 3A and B) that is more than 100 m deep and terminates at the northern end of a prominent morpho-bathymetric high (PMH, Figs. 2 and 3A,B).

The sedimentary wedge is bounded to the south by a steep, NE-SW oriented escarpment that is over 15 km long and up to 150 m high and incised by channels (Figs. 2 and 3A and B; bathymetric profile 3 in Fig. 2). Turbiditic levees are visible in the northern part of the continental rise. They consist of broad, kilometer-long ridges separated by channels up to 50 m deep (Figs. 2 and 3A).

The PMH of the northern continental rise, which extends over 25 km, is characterized by landslide scars and an asymmetrical shape (Figs. 2 and 3B, bathymetric profile 4). An arcuate seafloor depression surrounds its northern flank, probably formed by the action of bottom currents (current-eroded moat), which separates the PMH from a sedimentary body over 20 km long with the same shape, interpreted as sediment drift (e.g. Ref<sup>30</sup>). and affected by an 8 km wide landslide scar (Figs. 2 and 3A).

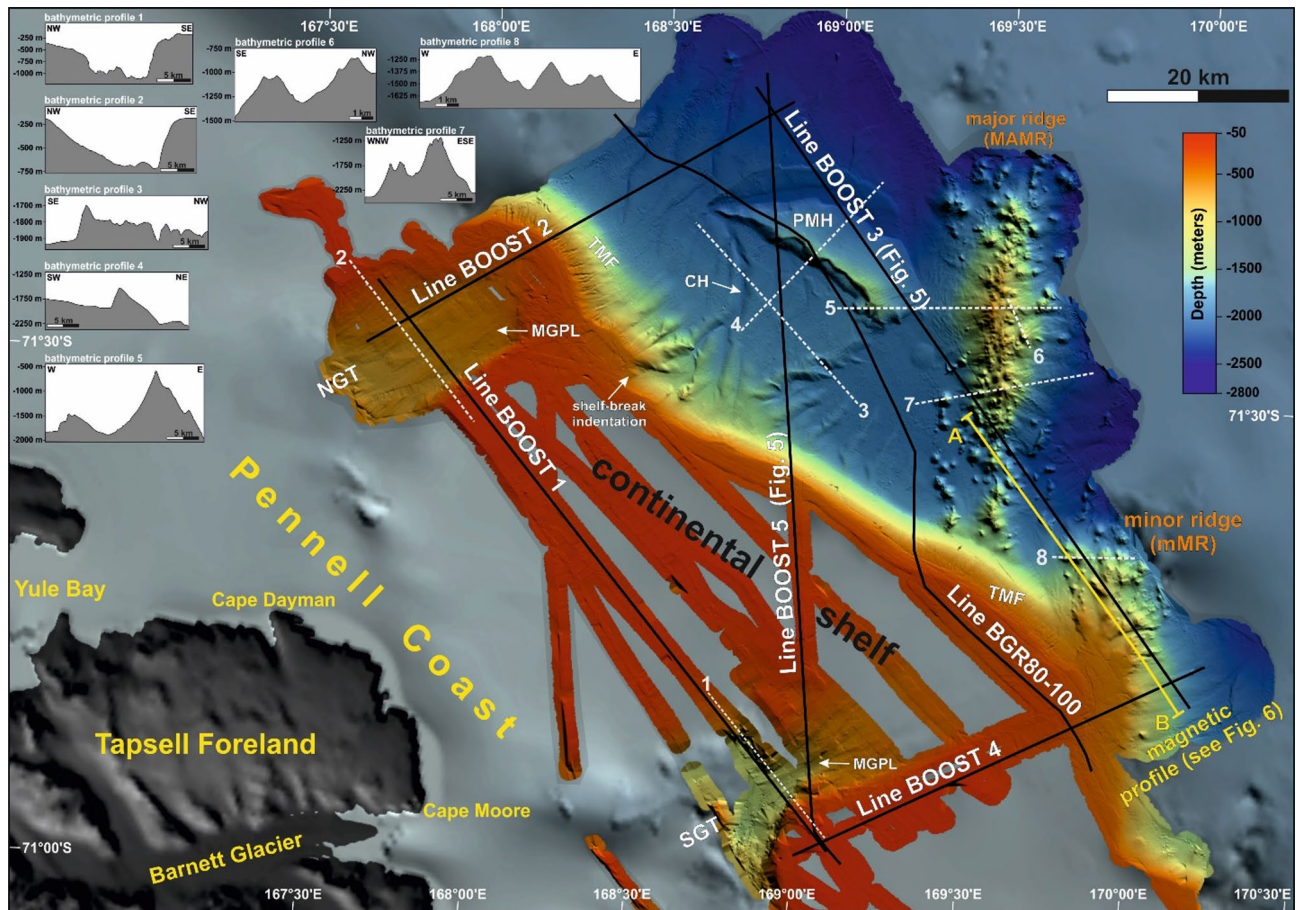


**Fig. 2.** Morpho-bathymetric map of the area covered by the multibeam data collected in the BOOST Project along the Pacific side of northern Victoria Land. The BOOST morpho-bathymetric data are superposed onto the digital bathymetric and topographic model of IBSCO<sup>24</sup> to fill the areas not covered by the BOOST data. The black segments indicate the five BOOST multichannel seismic lines, while the seismic profile BGR80-100 shows a non-linear trend (processed seismic data of Cruise BGR80 1980 is available at: <https://resource.bgr.de/describe/?url=https%3A//resource.bgr.de%2FMetadata%2FDataset%2F68d180de-f9c6-242f-e8d8-716bba000a36&graph=https%3A//resource.bgr.de/Metadata/&distinct=0>).

The dotted white segments show the traces of the eight bathymetric profiles reported in the top left of the figure, which cross the main morpho-bathymetric features of the area. The yellow segment is the marine magnetic profile (AB) acquired along the southern part of the line BOOST 3. Abbreviations: CH, major channel of the study area; NGT, north glacial trough; MGPL, mega-scale parallel lineations; PMH, prominent morpho-bathymetric high; SGT, southern glacial trough; TMF, trough mouth fan. The morpho-bathymetric map of Fig. 2 was created with the software Global Mapper, version 18.2.2, Blue Marble Geographics ([www.globalmapper.it](http://www.globalmapper.it)).

The southern sector of the continental rise is characterized by two broad, linear ridges that are roughly oriented in a north-south direction. The major ridge (MAMR) extends for over 45 km and is 10 km wide, with elevations reaching up to 1600 m above seafloor. The minor ridge (mMR) is at least 16 km long and 12 km wide, with elevations of up to 800 m. Both ridges consist of cone-shaped seamounts with subcircular or horseshoe-shaped craters on their summits (Figs. 2 and 3; bathymetric profiles 5, 6, 7 and 8 in Fig. 2).

Finally, it is important to emphasize that there is a considerable difference between the resolution of the bathymetric data acquired in the BOOST project and the data published in IBSCO<sup>24</sup> as shown in Fig. 4.

### Seismo-stratigraphic framework

Given the location of the study area at the northwestern end of the Ross Sea, the main unconformities identified along the acquired seismic lines in the Cenozoic sedimentary sequence were tentatively correlated with those recognized at DSDP (Deep Sea Drilling Project) Site 274 (250 km NNE of Cape Adare)<sup>31,32</sup> and in particular with the six Ross Sea unconformities (RSU1-6) identified by the Antarctic Offshore Acoustic Stratigraphy (ANTOSTRAT) project<sup>40</sup> (Fig. 4), and later additions (e.g. Refs<sup>41-44</sup>). The origin of the Ross Sea unconformities includes tectonic events, climate and ice sheet variations (e.g. Refs<sup>36-38</sup>). (Fig. 5).

The detection of the main unconformities is based on reflection terminations such as onlap, downlap and truncation, as well as on the separation between seismic units characterized by distinctive seismic facies.

Four Cenozoic unconformities were identified and labelled U4 to U1 from the oldest to the youngest (Figs. 5 and 6). The U1 to U3 unconformities were correlated with major climatic events, while the U4 unconformity was associated with the final separation between the Antarctic and Australian margins that occurred around the Eocene-Oligocene boundary (Fig. 5), in the sector linking NVL and Tasmania, and the onset of the ACC.

The high-amplitude U4 reflector is interpreted as the top of the breakup sequence (BS) (e.g. Refs<sup>39,40</sup>), which consists of seaward-dipping, semi-transparent to locally high-amplitude, high-frequency, discontinuous reflectors (seismic facies SF1 in Fig. 5) likely associated with the opening of the Tasman Gateway and thus dated to the late Eocene-early Oligocene. The BS generally exhibits a variable type of sedimentation, with mass-wasting deposits at the base topped by hemipelagic and fine turbidites and is seismically associated with an overlapping sequence (e.g. Ref<sup>40</sup>).

The drift sequence (DS) associated with the activation of the ACC lies with onlap terminations on the U4 and includes the U3 and U2 unconformities (Fig. 6). This sequence is seismically characterized by an alternation between high to low amplitude seismic packages thinning towards the continental slope, and consists of slightly seaward-dipping, high frequency, parallel and generally continuous reflectors (seismic facies SF2 in Fig. 5).

The U3 unconformity is identified in the central part of the DS within a thin seismic package consisting of high-amplitude reflectors separating two thicker seismic sequences made of low-amplitude reflectors (Fig. 6). U3 is locally characterized by onlap relationships with the overlying sequence and truncates the underlying sediments.

This surface can be associated with the mid-Miocene onset of the restoration of a polar-glacial regime (Fig. 5), marked by significant cooling of the Southern Ocean and the expansion of the Antarctic ice sheet, following the Miocene Climate Optimum (~17–14.6 Ma) and the Middle Miocene Climate Transition, ~14.6–13.9 Ma (e.g. Refs<sup>41–43</sup>). In particular, the U3 unconformity approximately corresponds to RSU4, which is dated to ~14.6–15.8 Ma<sup>44</sup>. The U2 unconformity, located in the upper part of the DS, marks the base of a well-layered seismic unit that extends to the seafloor and consists of continuous, high frequency, low- to high-amplitude reflectors (Fig. 6). The U2 is not identified along the continental shelf, while it can be tentatively interpreted along the continental slope (Fig. 6). This unconformity, which roughly corresponds to RSU2, is associated with the end of the Mid-Pliocene Warm Period (~3–3.3 Ma) (Fig. 5), when parts of Antarctica and notably West Antarctica were not covered by ice<sup>45–47</sup>.

The youngest unconformity U1 is only recognized on the continental shelf at the base of a thin sequence that reaches the seafloor (Fig. 6). This high-amplitude surface truncates the underlying reflectors and shows downlap and onlap relationships with the overlying deposits (Fig. 5). It has similar characteristics to the RSU1 unconformity identified by Granot et al.<sup>6</sup> on the southern continental shelf of the Adare and Northern basins. U1 approximately corresponds to RSU1 (Fig. 5), and a Pleistocene age of ~0.7 Ma is associated with this unconformity<sup>31,48</sup>.

Other key reflectors identified along the seismic lines are: (i) the top of the continental crust (CC); (ii) the top of the potential continent-ocean transition (COT); (iii) the top of the pre-rift deposits (Fig. 6).

The top of the CC was recognized on the structural high in the northern part of the continental rise as a faulted, undulated, discontinuous reflector with low- to high-amplitude (Fig. 6). The CC shows an opaque seismic facies with a chaotic aspect and local incoherent low- to high-amplitude internal reflections (seismic facies SF3 in Fig. 5). The top of the COT is a composite faulted seismic package consisting of discontinuous, low- to high-amplitude reflectors with contorted to chaotic geometry (Fig. 5). The COT seismic facies consists of discontinuous low- to high-amplitude reflectors with no internal coherence, possibly representing a stretched and thinned transitional crust made of a mixed volcano-sedimentary sequence (seismic facies SF4 in Fig. 5).

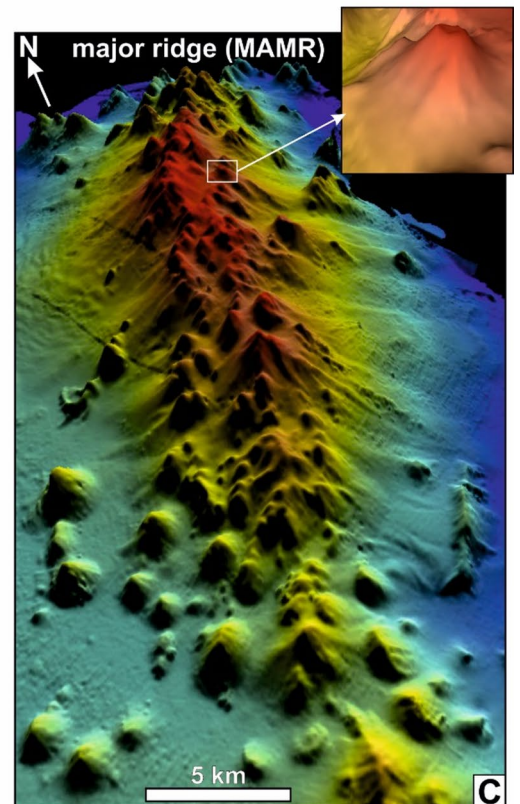
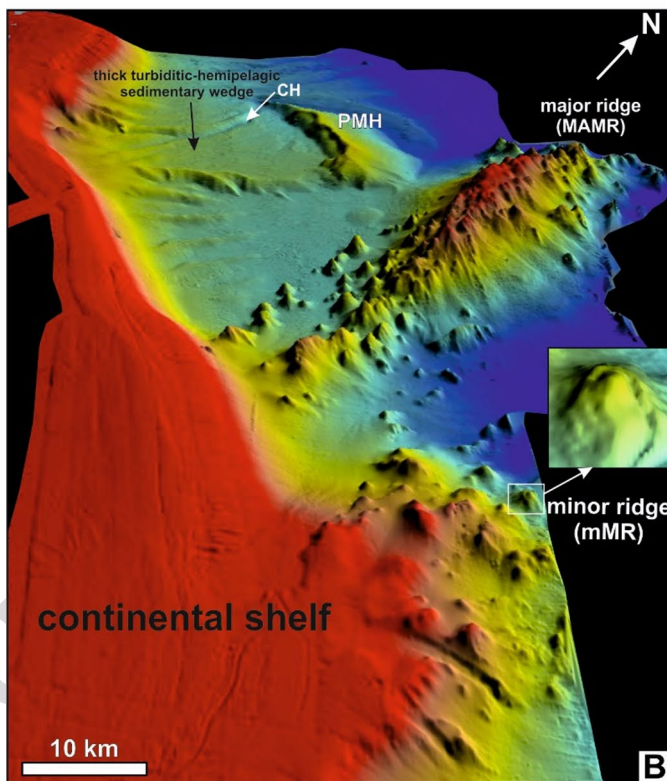
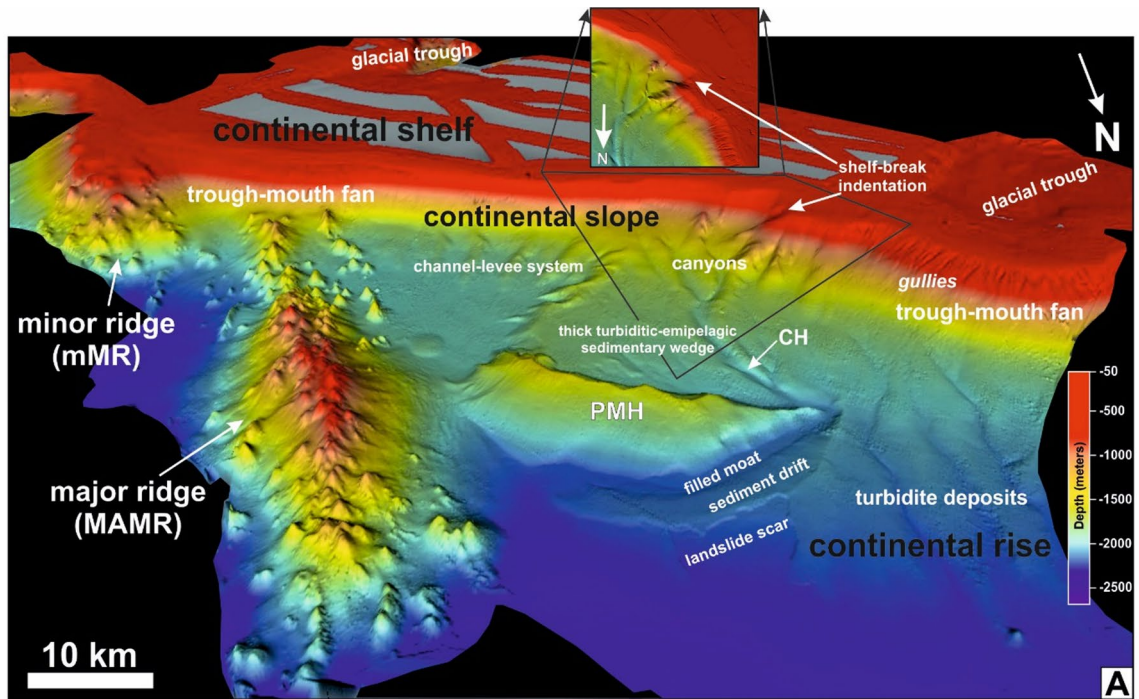
The erosional unconformity at the top of the pre-rift deposits is visible as a continuous high-amplitude reflector in the upper part of the structural high (Fig. 6). The pre-rift deposits exhibit chaotic-to-poorly stratified semi-transparent seismic facies consisting of low- to medium-amplitude, high frequency reflectors (seismic facies SF5 in Fig. 5). Finally, two additional seismic facies were identified, associated with the continental slope and seamounts that form the two ridges visible in the study area (seismic facies SF6 and SF7 in Fig. 5).

### Seismic line interpretation

The BOOST 3 and 5 seismic lines (Fig. 6) provide a good example of the seismo-stratigraphic setting and the main structural features of the study area. In addition, the line BOOST 3 is the only one crossing the two N-S oriented ridges identified by the morpho-bathymetric data (Figs. 2 and 6). Five seismic units were identified, including continental crust (CC), transitional crust (COT), pre-rift deposits, breakup sequence (BS), and drift sequence (DS).

#### Seismic line BOOST 3

The NW-SE oriented line BOOST 3 (Fig. 6) crosses the easternmost part of the study area (Fig. 2), along which a northern and a southern sector with different features can be recognized. The northern sector, which is characterized by very good seismic signal penetration (up to 5 s TWT), comprises a deep-sea zone down to 2300 mbsl and the prominent morphological high identified by the multibeam data (PMH). The basinal area consists of a well-layered DS that is up to 1.2 s TWT thick and consists of turbidite and contourite drift deposits gently dipping to the NW. The part of this sequence that lies between the basal Early Oligocene U4 unconformity and the Late Pliocene U2 unconformity thickens to NW. The reflectors show onlap terminations against the U4 unconformity and modest folding (drag folds, see inset A in Fig. 6) along the faults bounding the PMH structural high. The Late Pliocene-Quaternary uppermost part of the DS is up to 0.3 s TWT thick and shows onlap relationships to the SE against the U2 unconformity. The DS overlies the wedge-shaped BS, which is up to 0.6 s TWT thick in its SE part and consists of upward concave-shaped discontinuous reflectors truncated by the U4 unconformity. The inclination of the reflectors gradually increases towards the structural



high. The high-amplitude, contorted reflectors within the BS could be associated with the presence of mass-wasting deposits. The BS lies on a seismic unit characterized by a highly articulated top morphology formed by several fault blocks. This is interpreted as possible evidence for a COT that was stretched and thinned during the rifting phase. The structural high consists of an acoustically impenetrable seismic facies associated with CC. This isolated crustal block (CB), which coincides with the PMH shown in Fig. 2, is bounded by buried extensional faults that were active at least until the Middle Miocene, as indicated by the induced drag folds observed in the DS. The buried fault that bounds the CB to the south (SF fault in Fig. 6) may have a significant strike-slip component along which the CC is in contact with the Neogene sedimentary succession of the basin between the CB and the MAMR. The CB is covered by a thin (up to 0.25 s TWT in its central part), well-layered sedimentary mounded body containing the U2 unconformity and interpreted as a sediment drift.

◀ **Fig. 3.** The 3D views of the BOOST morpho-bathymetric data. **(A)** 3D view from NNE showing the major morpho-bathymetric features. The continental shelf is crossed by two glacial troughs located at both ends. The shelf-break is characterized by trough mouth fans adjacent to the glacial valleys and a prominent indentation (see the inset at the top). An isolated, NW-SE oriented, prominent morpho-bathymetric high (PMH) with a summit at 1400 mbsl is visible in the northern part of the continental rise. Between the PMH and the slope is located a thick sedimentary wedge of triangular shape bounded by steep scarps. The southern part of the continental rise includes two broad, roughly N-S oriented ridges of magmatic origin: the major ridge (MAMR) and the minor ridge (mMR). **(B)** 3D view from SE showing the asymmetrical shape of the PMH characterized by a steeper and shorter SW flank, and the 15 km long, 150 m high escarpment that bounds the thick sedimentary wedge to SE. A small basin that narrows towards the NE is located between the sedimentary wedge and the MAMR. The MAMR has a maximum height of 1600 m above the seafloor in its central part, where the summit lies at 550 mbsl. The mMR appears to merge with the continental shelf at its southern end. Its maximum height is 800 m above seafloor and reaches a minimum of 750 mbsl. It consists of cone-shaped seamounts and small ridges. The tops of several seamounts exhibit subcircular craters or horseshoe-shaped craters that may contain secondary cones (see inset on the left). **(C)** 3D view of the major ridge (MAMR) from SSW. It consists of hundred meters high individual cone-shaped seamounts and small ridges of coalescing seamounts up to 3 km long with sharp summit and variable orientations from NE-SW to NNW-SSE. The northern and southern ends of the MAMR are mainly formed by scattered seamounts and ridges, while the central part corresponds to a swell mainly consisting of ridges at the top. Several seamounts show subcircular (see inset top right) or horseshoe-shaped craters at the top. The 3D views of the BOOST morpho-bathymetric data of Fig. 3 were created with the software Global Mapper, version 18.2.2, Blue Marble Geographics ([www.globalmapper.it](http://www.globalmapper.it)).

The basin between the CB and the MAMR shows a considerable thickening of the uppermost part of the DS, which shows Late Pliocene-Quaternary deposits up to ~0.6 s TWT thick and with onlap terminations against the U2 unconformity. The Miocene unconformity U3 was not identified. Here, the well-layered seismic facies associated with the DS is disturbed by the presence of a sub-vertical body interpreted as magmatic rise generating a young volcano, as well as two buried, overlapping landslide deposits (Fig. 6 and inset B). In addition, two mound-shaped bodies, characterized by semi-transparent chaotic internal reflectors, a convex top and potential magmatic sills at the base, are located below the landslides and above the Late Pliocene U2 unconformity (Fig. 6 and inset B). They were interpreted as possible hydrothermal vent complexes (HTVC in Fig. 6) formed by the upward migration of gases and fluidised material associated with the emplacement of magmatic sills (e.g. Refs<sup>49-51</sup>).

The BOOST 3 line crosses the MAMR for ~9 km at the southern end of its central bulge, which consists of a sequence characterized by chaotic seismic facies in which potential vertical conduits feeding volcanoes can be recognized. Numerous recent volcanic cones of varying elevation and near each other can be seen on the seafloor (Figs. 3 and 6). The largest cones are in the central part of the ridge, where a minimum water depth of 1400 mbsl is reached. Some normal faults affect the MAMR. The southeastern volcanic cones show semi-transparent layered seismic facies, possibly due to the presence of an alternation of lavas, pyroclastic and inter-eruptive sedimentary deposits. In the filling of the basin between MAMR and mMR, the main unconformities are not recognizable, except for the possible U2 surface along the margins. An evident magma ascent that has produced a volcanic cone is visible in the south-eastern part of this basin. Instead, the small cone in the central part is the result of lateral reflections. In addition, two dome-shaped bodies ~5 km long and up to ~0.4 s TWT thick, characterized by a semi-transparent chaotic seismic facies, are visible near the seafloor beneath a thin sedimentary cover. They appear to be fed by vertical conduits consisting of low amplitude chaotic reflections. Based on this evidence, these bodies could be HTCVs. Possible strata-concordant sills, which are highlighted by the presence of high amplitude reflectors (e.g. Refs.<sup>50,52</sup>), have been interpreted at depth of ~3.8 s TWT.

The mMR is crossed by the line BOOST 3 for ~16 km. It consists of a prominent, smooth relief with a minimum water depth of ~800 m along which several recent volcanic edifices are visible. This ridge does not appear to consist entirely of magmatic rocks, as it is interrupted by sedimentary sequences. Finally, a series of possible magmatic intrusions characterizes the southeasternmost part of the seismic line (Fig. 6). The magmatic intrusions consist of narrow zones with chaotic acoustic character or convex-upward reflectors that interrupt the continuity of the seismic reflections that can be tilted around this intrusion. These features are also clearly visible in the buried part of the young volcanoes indicated in Fig. 6.

#### *Seismic line BOOST 5*

The N-S oriented line BOOST 5 (Figs. 2 and 6) crosses a broad part of the continental shelf along which the seismic penetration is low (less than 0.5 s TWT). It consists of glacial depositional systems characterized by a sub-horizontally layered sequence in the inner part and by prograding reflectors to the outer shelf. A distinct cross-shelf glacial trough has incised the southern part of the shelf. The Late Pleistocene U1 erosional unconformity is visible along the entire shelf and ends at the shelf-break. It has eliminated part of the Pliocene to Quaternary sequence as evidenced by the toplap termination of the late Pliocene U2 unconformity against this overlying erosional surface. The Middle Miocene U3 unconformity is clearly recognizable along the outer shelf and represents the base of a prograding seismic unit. The continental slope consists of seaward prograding reflectors, including the U2 and U3 unconformities, which form a thick (over 0.6 s TWT) wedge-shaped glacial sedimentary sequence that developed between ~600 and ~1800 mbsl. The northern part of the line crosses the CB, which, as seen in line BOOST 3, is bounded by a series of buried normal faults and is surrounded by the

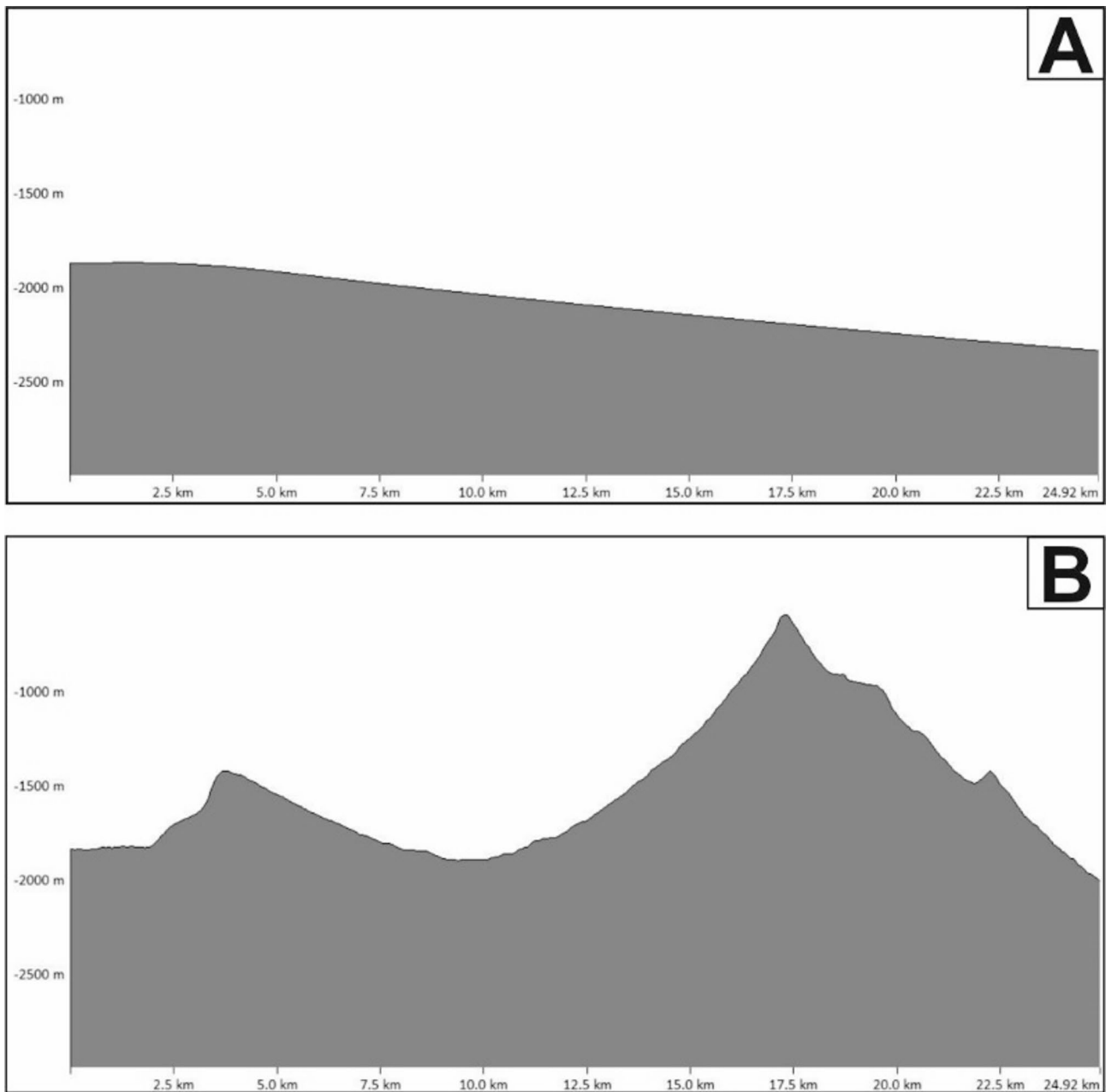


**Fig. 4.** Difference between BOOST and IBSCO bathymetry data. There is a considerable difference between the bathymetric data acquired in the BOOST project and those published in IBSCO<sup>24</sup>. This difference is illustrated by the comparison between two matching bathymetric profiles: IBSCO data in A and BOOST data in B (bathymetric profile 5, location in Fig. 2).

wedge-shaped BS. BS lies on a faulted transitional crust (COT) on the southwestern and northern flanks of CB. A thick (~1.25 TWT) DS rests on the BS showing onlap terminations against the U4 unconformity.

The tectonic activity of the main fault bounding the northern side of CB seems to be sealed by the U2 unconformity, as indicated by the modest folding (drag folds; see inset C in Fig. 6) of the reflectors at the fault planes. This indicates that the fault was probably active until the Pliocene. A Pliocene-Quaternary tectonic activity of the main fault at the southeastern boundary of CB can be inferred both from the evidence that the U2 unconformity and DS are cut by the fault plane and from the presence of a steep scarp characterizing this side of CB (see Figs. 2, 3B and 6).

In addition, it is possible to observe the presence of a thin (up to 0.25 TWT) sedimentary cover on the top of the CB, interpreted as pre-rift deposits of uncertain age.

The northern part of the basin, situated between the CB and the continental slope, exhibits distinct characteristics that differ from those observed in the southern part. Here, the BS sequence and the COT are not visible, while the DS is thickened, as previously observed along the line BOOST 3. However, here the thickness

of the Late Pliocene-Quaternary sequence is constant, while the Middle Miocene-Pliocene part of the DS is thickened. It is inferred that the two parts of this basal area may be separated by the western extension of the SF fault, which is located at the southeastern end of the CB along line BOOST 3. This tectonic structure, which deformed the BS, the COT and partially the drift sequence, may have a significant strike-slip component, as suggested by the abrupt contact between sequences of different ages visible across the fault. Notably, a possible right-lateral component of movement along the SF and a Quaternary activity cannot be excluded, as it appears to control the observed shelf-break indentation (Figs. 2 and 3A). Finally, this basin is characterized by the widespread occurrence of sub-vertical, narrow, low-amplitude chaotic features interpreted as pipes associated with vertically focused fluid flows.

### Marine magnetic data

The magnetic profile AB, which runs parallel to the southern part of the seismic line BOOST 3 with a horizontal offset of 1.3 km to the south-west (Fig. 2), is shown in Fig. 6. This deviation influences the magnetic anomaly along the MAMR as the profile crosses its southern end, which consists of scattered volcanic cones rather than the main magmatic body, as is the case for line BOOST 3. Marine magnetic data are often helpful for discriminating the magmatic affinity of outcropping or buried geological bodies. The magnetic anomaly profile shows the presence of two distinct peaks associated with the two recognized magmatic ridges. The northern magnetic anomaly peak is associated with the MAMR. It is broad, symmetrical and has higher amplitude values, in contrast to the southern peak associated with the mMR, which is narrower and sharper. In addition, it does not encompass the entire mMR crossed by the line BOOST 3 and shows an asymmetric shape with a maximum positive value of ~290 nT along the SE part and negative values up to over -180 nT along the NW part, probably related to the presence of zones composed of sedimentary sequences. The steep gradient on both sides of the anomaly associated with the mMR could be related to a localized or shallow magmatic source. The bell-shaped peaks associated with the MAMR cover the entire ridge with values between 100 and 330 nT. The highest value is located along the southern continuation of the axis of the MAMR and could indicate the deep termination of the largest magmatic body visible along line BOOST 3. The higher values also include a large part of the basin between the two magmatic ridges. The broad magnetic anomaly associated with the MAMR suggests the presence of a deep magmatic source.

### Aeromagnetic data

Aeromagnetic data are a useful tool to identify anomalies at a regional scale. The gridded aeromagnetic data acquired during the BGR-expedition GANOVEX IX in 2005-06 covers the area of the BOOST bathymetric and seismic survey and extends beyond the study area<sup>53</sup> (Fig. 7A). A prominent pattern of high-frequency anomalies can be traced from Coulman Island, the Daniell Peninsula, the Hallett Peninsula and especially the Adare Peninsula further along the shelf into the BOOST survey area (Fig. 7A). Superposition of mapped volcanic rocks from the Hallett volcanic suite on each island perfectly matches the calculated analytical signal and provides an estimate of the complete outline of the magnetic source bodies (Fig. 7B). Within the survey area, this high-frequency signal is attenuated by a positive long wavelength magnetic anomaly associated with CB (Fig. 7C), whereas the analytical signal provides a much clearer response (Fig. 7D). The positive long wavelength anomaly is indicative of a deeper-seated magnetic source body, and its position corresponds well with the outline of the isolated CB seismically imaged along the lines BOOST 3 and 5 (Fig. 6). This anomaly was not described by Damaske et al.<sup>53</sup> but was later interpreted as a possible granitic body of Palaeozoic age and thus of continental crust origin<sup>20</sup>.

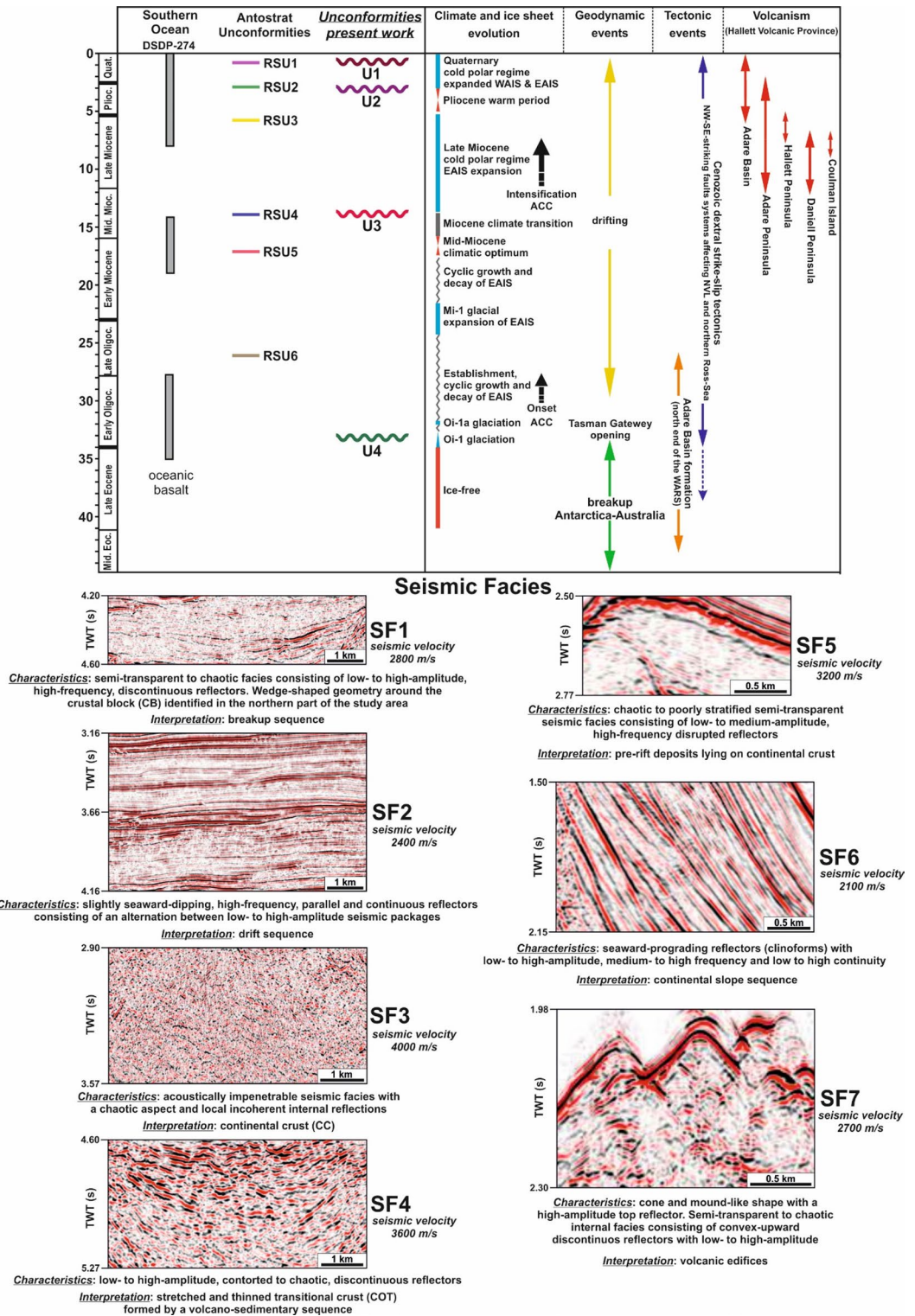
The bathymetric high of the mMR correlates more closely with the outlines of the magnetic bodies obtained by the analytical signal than the MAMR, which appears to be divided into two distinct parts (Fig. 7B, D). However, it is important to note that the resolution of the airborne magnetic data is not as high as that of the bathymetric data. Consequently, individual features such as craters and cones observed in bathymetry are not resolved in detail. In addition, the magnetic anomalies over the MAMR, which are rather patchy or indicate dissection, may be the result of the wide and sharply angled line spacing of the flight lines covering this ridge (Fig. 7C, D).

Damaske et al.<sup>53</sup> who had previously associated the high-frequency signal with rocks from the Hallett Volcanic Province, suggested that these extend north-northwestward across the continental shelf and slope at least 130 km into the ocean. However, the new bathymetric data allow the high-frequency anomalies to be assigned with greater clarity to the newly imaged magmatic ridges and separate linear volcanic centers, rather than a single one extending oceanward from Cape Adare.

### Discussion

In the present study, high-resolution multibeam data, bathymetric profiles and 3D views were used to analyze the seafloor characteristics of the Pacific coast of the NVL. The results were combined with the interpretation of new multichannel seismic reflection profiles, marine magnetic measurements and offshore aeromagnetic data to define the structural setting and geodynamic evolution (Fig. 8) of this underexplored area, which lies at the northern end of the East-West Antarctica boundary.

The continental shelf is incised by two ENE-WSW oriented glacial troughs, which terminate at the shelf-break with trough mouth fans (TMF; Figs. 2 and 3). These troughs have an asymmetrical profile with steep southern flanks, with the southern trough in particular showing an abrupt change in orientation. These features suggest a possible interaction between past ice streams and tectonics. Moreover, a network of incised gullies is visible on the northern TMF, indicating large volumes of meltwater at the base of the former ice tongue. These glacial morphologies highlight the considerable retreat of the glaciers in this area (several tens of kilometers from the coast).



Morpho-bathymetric and geophysical data revealed three prominent kilometer-scale features in the deeper part of the study area (Figs. 2 and 3). The northern one is a structural high of continental crust (CB in Figs. 6, 7 and 8) interpreted as a relict and rotated block formed during the continental rifting phase, which preceded the Antarctic and Australian plates breakup that started around the Eocene-Oligocene boundary (U4 unconformity, Figs. 5 and 6) and led to the opening of the Tasman Gateway. The CB is bounded by normal faults (Fig. 8A) that were probably active at least until the Pliocene (Fig. 6). The roughly E-W SF fault, which affects the southeastern end of the CB (Figs. 6 and 8) and deforms the shelf-break, shows clues of a younger right-lateral component of motion. A large positive long wavelength magnetic anomaly is located at the CB (Fig. 7) and can most likely be interpreted as a remnant of a Paleozoic granitic continental basement, e.g. Granite Harbour-type or Admiralty intrusives<sup>20</sup>.

◀ **Fig. 5.** Main Cenozoic unconformities and seismic facies identified along the BOOST seismic lines. Unconformities U4 to U1 identified along the BOOST seismic lines in the Cenozoic sedimentary sequence correlated and dated by the time-distribution of the DSDP-274 site stratigraphy, ANTOSTRAT Ross Sea Unconformities RSU6 to RSU1<sup>33–35</sup>. The variations in the Antarctic climate and ice sheet are reported as well as geodynamic and tectonic events recorded in the Ross Sea area (see text for references). The age of the volcanic fields forming the Hallett Volcanic Province<sup>9</sup> is also indicated. Seismic facies: Description of the seven seismic facies recognized in the multichannel seismic reflection profiles and their interpretation. The representative boxes are extracted from the seismic lines BOOST 3 and 5. Seismic facies SF1 and SF2 are associated with the Cenozoic sequences of breakup and drift, respectively, while SF3 and SF4 are associated with continental crust (CC) and transitional crust (COT), respectively, and SF5 with pre-rift deposits. Seismic facies SF6 is characterized by seaward-prograding reflectors that form the continental slope sequence, while SF7 is the seismic facies associated with the seamounts that form the MAMR and mMR and interpreted as volcanic edifices. The average seismic velocity of each box is also reported.

The southern sector of the study area is characterized by the presence of two roughly N-S oriented active magmatic ridges (MAMR and mMR in Figs. 2, 3, 6 and 8), which were identified for the first time as the CB.

The new detailed bathymetry presented in this study allowed a more accurate interpretation of the high-frequency aeromagnetic anomalies reported in previous studies of this region (e.g. Refs<sup>20,53</sup>). These anomalies were interpreted as the result of a single volcanic linear feature connecting with and extending at least 130 km oceanward from Cape Adare. The new data (Fig. 7) show that these anomalies are clearly associated with the two distinct magmatic ridges and with another offshore magmatic ridge north of Cape Adare (OCAMR in Figs. 7D and 8), which is also recognizable by morpho-bathymetric data (see Supplementary Material). They likely represent the extension of the alkaline magmatism recognized onshore at Daniell, Hallett and Adare peninsulas into the oceanic realm (Fig. 1). This indicates a close connection between on- and offshore structures at the coastal margin of NVL, which is clearly imaged by the superposition of the magnetic anomalies with the maximum horizontal gradient (MHG, Fig. 8B). The pronounced volcanic ridges exhibit a left-stepping en-echelon pattern (Fig. 8), a structural configuration associated with NW-SE trending right-lateral fault zones. Due to the genetic link between faulting and magmatic array, the timing of magmatism and right-lateral strike-slip kinematics should be coeval. A similar tectonic connection between N-S Neogene magmatic bodies and extensional structures within a NW-SE right-lateral fault zone has already been documented onshore of NVL<sup>3,20,56,57</sup>.

The geophysical data presented here show that the northern and southern sectors of the study area have recorded different tectonic events that occurred during the geodynamic evolution of the offshore NVL. The northwestern sector, where the rifted crustal block CB is located, has recorded the Cenozoic tectonic evolution since the Eocene-Oligocene boundary, which led to the opening of the Tasman Gateway. The seismic data allowed the identification of a thick drift sequence containing several unconformities (U1–U3, Figs. 5 and 6) related to climatic events and resting on the wedge-shaped breakup sequence, which in turn lies on transitional crust. During the initial phase of the opening of the Tasman Gateway, a NW-oriented, left-lateral transform plate boundary developed between the Antarctic and Australian margins (Fig. 8C), which caused NVL and Tasmania moving away from each other in the study area.

The south-eastern sector is formed by recent strike-slip tectonics, likely active since the Pliocene (e.g. Ref<sup>6</sup>)., which led to the formation of the two large magmatic ridges. These are thought to be associated with the development of roughly N-S oriented extensional faults that formed within a NW-trending, right-lateral megashear zone that extends from the oceanic region to the continental shelf and possibly includes the magmatic ridge located in the offshore of the Adare Peninsula (Fig. 8D). The rise of magma to the surface was also favored by the thinned continental lithosphere present in this part of NVL<sup>58,59</sup>.

The change in kinematics of pre-existing deformation zones is consistent with plate tectonic reconstructions of the SW Pacific region, particularly in the Tasmania-NVL sector, and reflects the rift-to-drift evolution between the Australian and Antarctic plates<sup>4,60,61</sup>. This plate tectonic reconstruction comprises three key stages (see Fig. 3 in Cande & Stock<sup>60</sup> and Fig. 34 in DeMets et al.<sup>61</sup>): (1) Late Cretaceous-Eocene (70–43 Ma)<sup>62</sup> during which this region experienced a slow seafloor spreading coeval with a left-lateral transform margin. There, this stage marks the rifting phase and the incipient drift between Australia and Antarctica; (2) Eocene to Oligocene (43–33 Ma), during this stage spreading rates increased, leading to the onset of seafloor spreading in the Adare Trough and the beginning of separation between the Australian and Antarctic plates in this sector; (3) 33–26 Ma, this period was characterized by rapid separation of the plates, cessation of the Adare Trough spreading and the onset of northward drift of the Australian plate along the Tasman-Balleny fracture zone corridor. In addition, Antarctica began to act as an independent plate (e.g. Refs<sup>4,10,63,64</sup>). This stage also marks a significant change in the tectonics of the SW Pacific (e.g. Ref<sup>4</sup>)., including the considerable southward migration of the Macquarie Triple Junction and the possible separation of the Macquarie Plate (e.g. Ref<sup>15</sup>). Moreover, a rotation of the direction of regional extension from ENE-WSW to ESE-WNW occurred, triggering right-lateral shear in the sector comprising the study area that is located within the Antarctic plate in the southward projection of the Tasman-Balleny fracture zone corridor (Refs. 3,10,60,61,63,64). In this context, the right-lateral megashear zone in conjunction with the thinning of the continental crust that developed in the study area during the Pliocene-Quaternary (Fig. 8E) fits well with the geodynamic evolution described above. This deformation zone could thus represent the intraplate continuation of the Balleny Fracture Zone (Fig. 1), as already proposed by several authors for NVL and the western Ross Sea (e.g. Refs. 3,18,64).

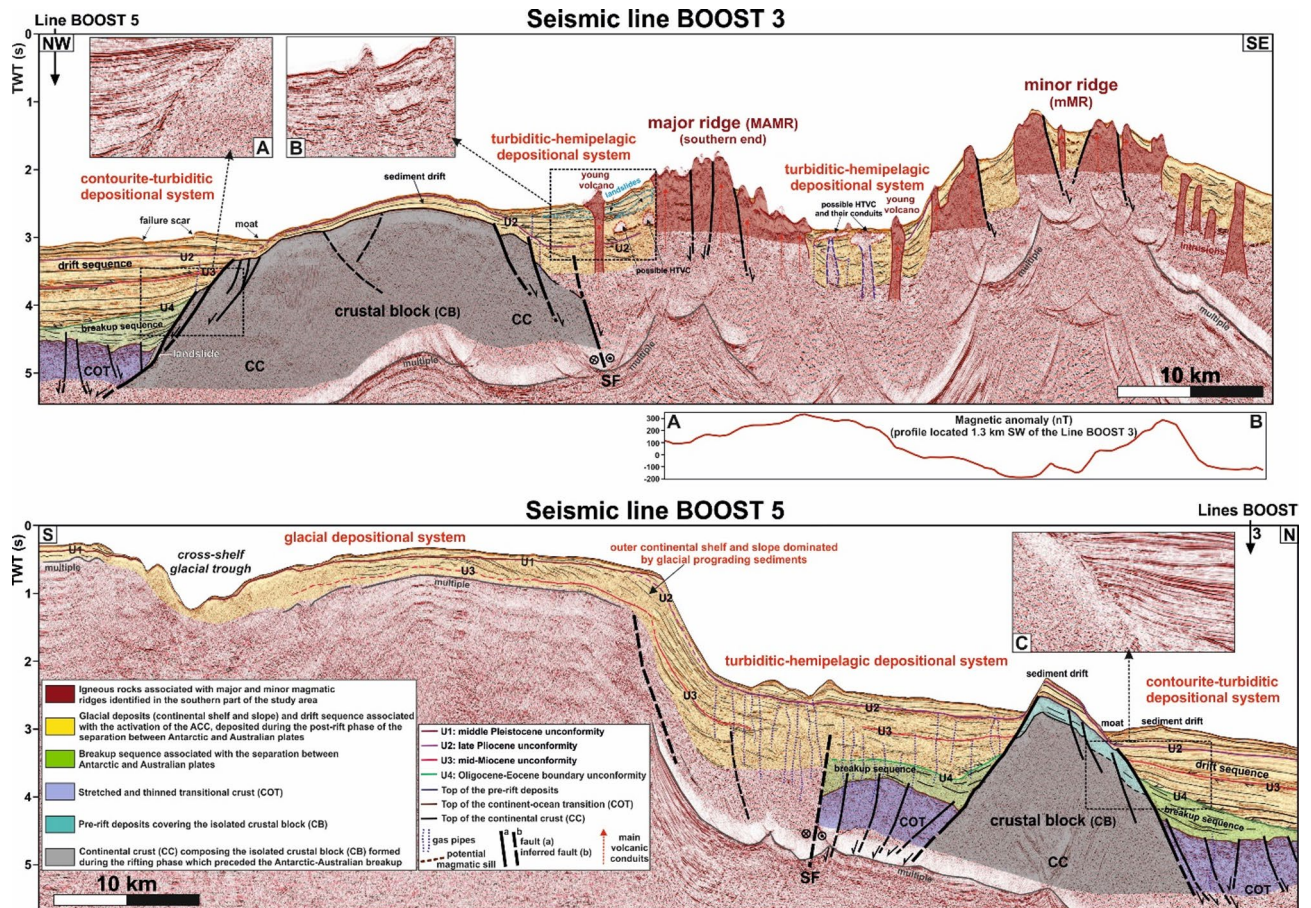


**Fig. 6.** Interpretation of the migrated seismic lines BOOST 3 and 5. Line BOOST 3 (position in Fig. 2) crosses the north-easternmost and deepest part of the study area, along which can be recognized from NW to SE: a basinal area filled by a breakup sequence overlying a thinned and faulted transitional crust (COT) and covered by a thick drift sequence mainly consisting of contourite and turbidite deposits; the isolated faulted crustal block (CB) of continental nature (CC) covered by a sediment drift; the two prominent major and minor ridges consisting of seamounts interpreted as volcanic edifices. Possible buried magmatic intrusions were also identified. The marine magnetic profile AB (position in Fig. 2) acquired along the south-eastern part of the seismic line BOOST 3 is also reported below the line. Insets A and B respectively show the drag folds along the fault bounding the CB to the north-west and a young volcano that crosses two buried landslide bodies. The marine magnetic profile AB, which was acquired along the southern part of the line BOOST 3, is also reported (see position in Fig. 2). Along the line BOOST 5 (position in Fig. 2) can be recognized: the southern and central part of the continental shelf, in which a V-shaped glacial trough is located; the continental slope, which consists of seaward glacial prograding sediments; the continental rise, which is divided into two basinal areas by the presence of the isolated faulted CB surrounded by transitional crust; the deepest and northernmost part of the line includes the same basinal area that was described along the line BOOST 3. It is inferred that the fault at the southeastern end of the CB (SF) along the line BOOST 3 may cross the central part of the basin between the CB and the continental slope visible along the line BOOST 5. This structure may have a significant strike-slip component of movement as an abrupt contact between sequences of different ages is visible across the fault, which could be also responsible for the indentation of the shelf-break (see Figs. 2 and 3A) characterized by a right-lateral displacement. Inset C shows the drag folds along the fault that bounds the CB to the north. Uninterpreted seismic profiles BOOST 3 and 5 are available in the Supplementary Material.

## Methods

The analyzed dataset consists of multibeam swath bathymetry data, multichannel seismic reflection profiles (MCS) and marine magnetic measurements acquired with the R/V OGS Laura Bassi and integrated by an offshore aeromagnetic survey of the NVL conducted by the BGR (Federal Institute for Geosciences and Natural Resources).

A total of ~4290 km<sup>2</sup> of seafloor were mapped with a Kongsberg EM304 multibeam echosounder system (512 equidistance-beams, operative frequency of 30 kHz). The morpho-bathymetric data were processed using QPS Qimera software considering variations in sound velocity and applying quality control. The resulting Digital Terrain Model (DTM), with a grid cell size of 50 × 50 m, was edited (removal of residual spikes) and filtered. Data visualization and interpretation was done using the GlobalMapper<sup>®</sup> software from Blue Marble Geographics.

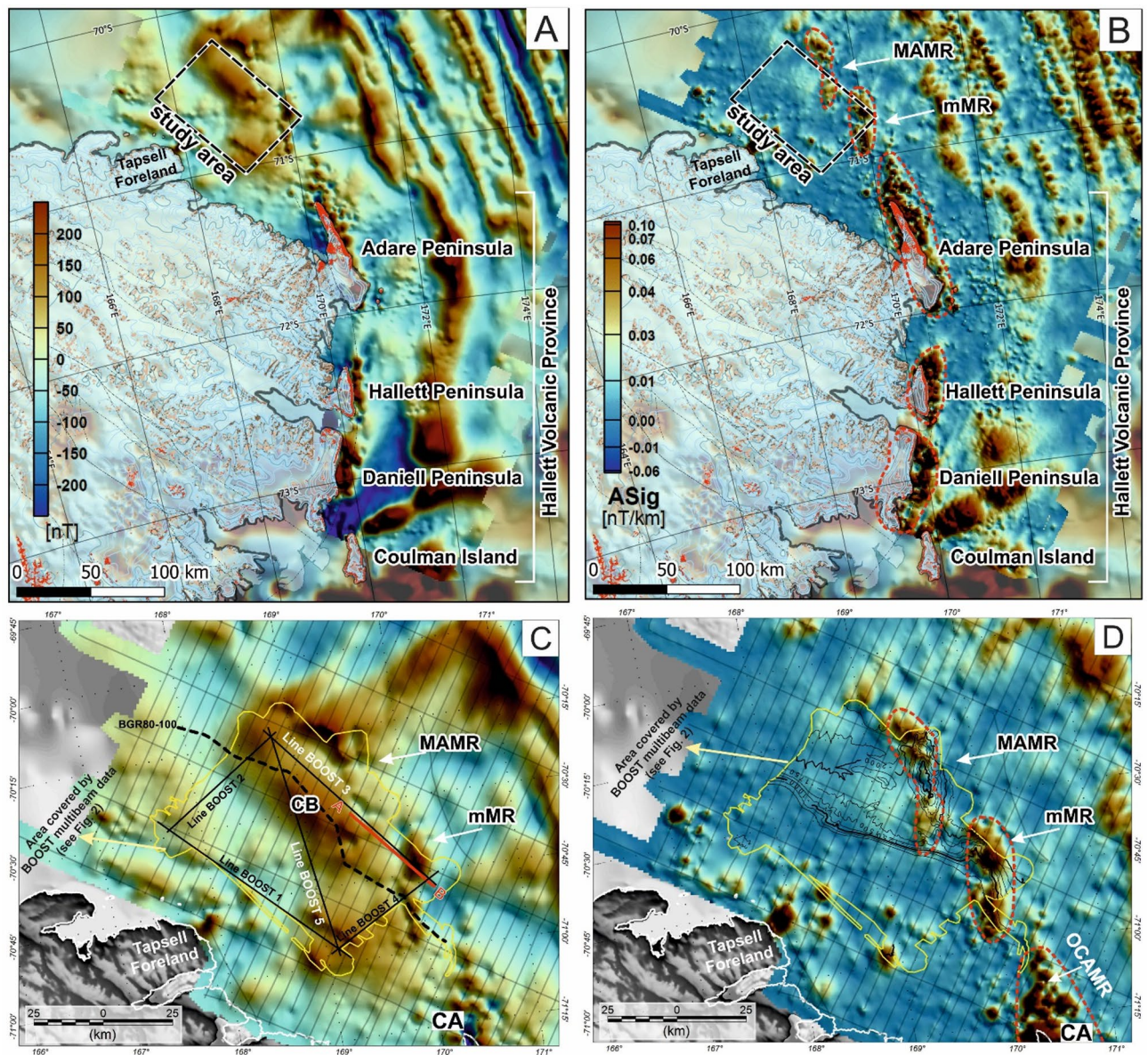


**Fig. 7.** Aeromagnetic data. Overview of the aeromagnetic anomaly data<sup>53</sup> superimposed on ADMAP-2 data onshore<sup>54</sup> and close-up maps of the study area. (A) Magnetic anomaly map of northern Victoria Land and highlighted red outline of exposed rocks of the Hallett Volcanic Province at Coulman Island and the Daniell, Hallett and Adare peninsulas (GeoMAP<sup>55</sup>). (B) Analytical signal of the magnetic anomaly data. The dashed red lines refer to the interpreted causative magnetic sources. The outlines align reasonably well with the mapped volcanic units and can be traced offshore into the BOOST survey area. Note the slightly different orientation and dissection of the causative magnetic sources representing distinct volcanic ridges. (C) Close-up of the magnetic anomaly map of the study area: The high frequency magnetic anomaly signal corresponds to the major ridge (MAMR) and minor ridge (mMR) of magmatic origin and the northern tip of the Adare Peninsula, that is Cape Adare (CA), and is attenuated by a positive long wavelength anomaly associated with an isolated crustal block (CB; colorbar as in A). The red segment is the marine magnetic profile AB acquired along the southern part of the line BOOST 3 (see Fig. 6). (D) The close-up of the analytical signal map shows the imaged causative source bodies (red dashed outlines) that align with the newly mapped MAMR and mMR, as indicated by the black counter lines of the bathymetric survey (colorbar as in B). An offshore magmatic ridge (OCAMR) is visible at the northern tip of Cape Adare (CA). The maps of Fig. 7 were generated with the geophysical software “Oasis montaj”, version 2023.1, ([www.seequent.com/products-solutions/oasis-montaj/](http://www.seequent.com/products-solutions/oasis-montaj/)).

Five multichannel seismic profiles with a total of 353 km were acquired using a source consisting of 2 GIGuns (i.e., TRUE-GI mode with a volume of 300 inch<sup>3</sup>) and a 1500 m-long streamer with 120 hydrophones (i.e. Sercel Seal 428 system). A pre-stack Kirchhoff time migration was applied to all seismic lines in order to correctly image the geometries of the reflectors. The techniques used to remove the multiples, also to preserve

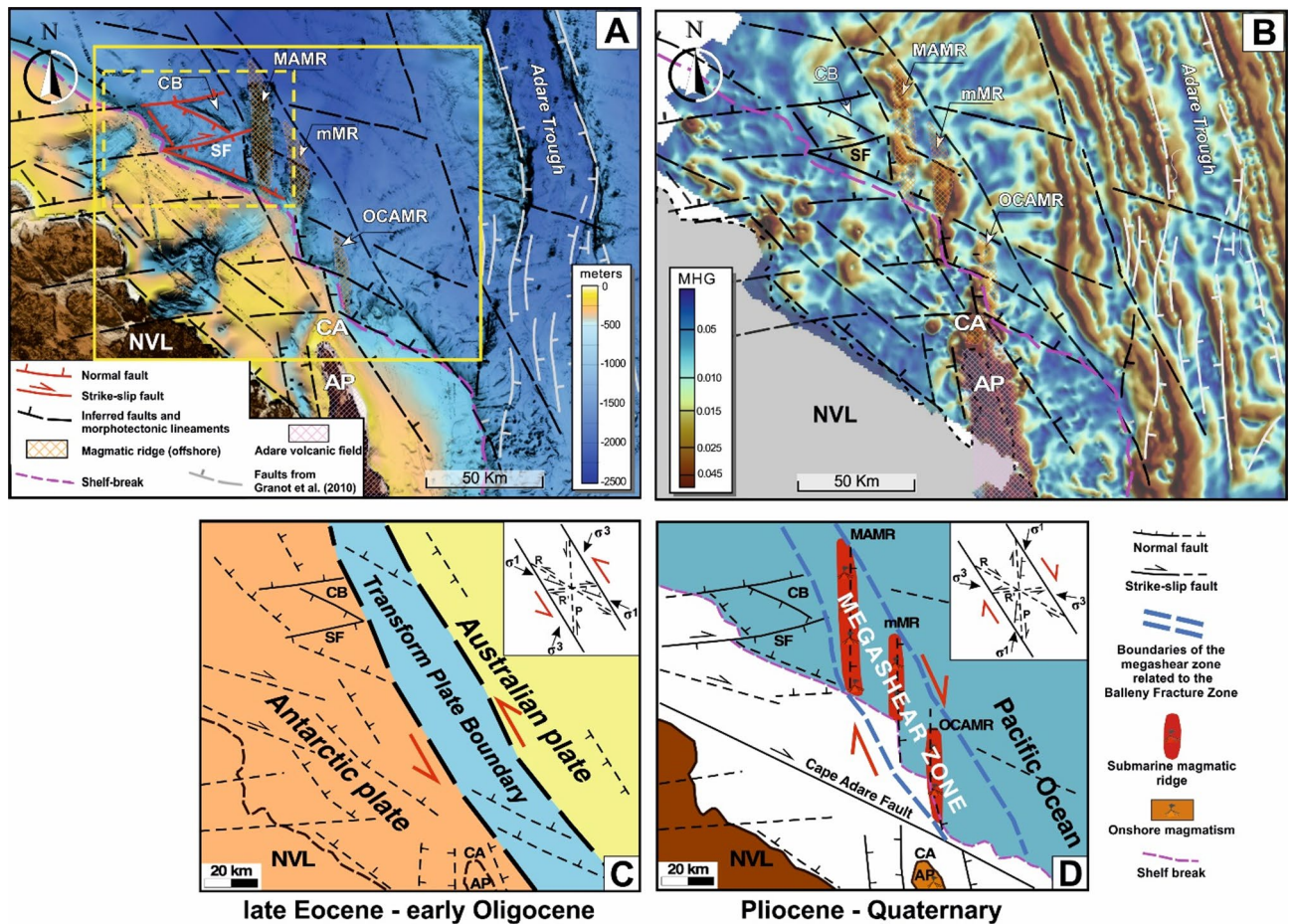


**Fig. 8.** Tectonic map and geodynamic models of the study area. (A) Simplified structural map of the study area (dashed yellow box) and the surrounding regions. Faults identified in the present work by multichannel seismic lines and multibeam data are shown in red; in black are the inferred faults and morphotectonic lineaments derived from the analysis of the multibeam data and the DEM created with GMRT, version 4.3.0 ([www.gmrt.org](http://www.gmrt.org)), and the software GeoMapApp, version 3.7.4 ([www.geomapapp.org](http://www.geomapapp.org); CC by Ryan et al.<sup>22</sup>) and integrated with literature information<sup>4,21</sup>; in grey the faults of the Adare Trough by Granot et al.<sup>6</sup>. The submarine magmatic ridges identified in this work (MAMR and mMR) are also shown, together with the magmatic ridge (OCAMR) north of Cape Adare (CA), which was recognized on the basis of aeromagnetic and morpho-bathymetric data (see Supplementary Material). The map of (A) was created with Global Mapper, version 18.2.2, Blue Marble Geographics ([www.globalmapper.it](http://www.globalmapper.it)), and Geo-Suite AllWorks, version 2024R1, Geo Marine Survey Systems ([ww2.geosys.nl/en/software/geosuite-allworks](http://ww2.geosys.nl/en/software/geosuite-allworks)). (B) Tectonic structures and magmatic ridges in (A) superimposed on the maximum horizontal gradient of the aeromagnetic anomaly data. In general, the maximum value of the horizontal gradient is theoretically located above the edge of its potential source and enhances the edges of the magnetic anomaly data to identify the boundaries of its source. The maximum values indicated by red colours provide an approximate outline of the potential source bodies, which align well with the mMR and MAMR. The map of (B) was generated with the geophysical software “Oasis montaj”, version 2023.1, (<https://www.sequent.com/products-solutions/oasis-montaj/>). (C) Simplified geodynamic reconstruction of the area shown in (A) (yellow box) during the late Eocene-early Oligocene, when the initial phase of the opening of the Tasman Gateway was likely characterized by the development of a NW-oriented, left-lateral transform plate boundary between the Antarctic and Australian margins. (D) Simplified geodynamic reconstruction of the area shown in Fig. 8A (yellow box) during the Pliocene-Quaternary. The magmatic ridges (MAMR, mMR, OCAMR) are associated with the development of roughly N-S oriented extensional faults that formed within a NW-trending, right-lateral megashear zone. This deformation zone is thought to be the result of intraplate continuation of the Balleny Fracture Zone in the offshore area of northern Victoria Land. The megashear zone reactivated the former plate boundary. AP Adare Peninsula, CB crustal block, NVL northern Victoria Land, SF buried fault at the south-eastern end of the CB.

the primary reflections, allowed to remove them only partially. The use of migration therefore produced diffractions in the multiples that, although not aesthetically pleasing, do not affect the interpretation of the data. Processing was performed using the open-source seismic processing package Seismic Unix and Echos™ software from Aspentech. The seismic interpretation was performed using the S&P Global Kingdom seismic package.

The magnetic survey was carried out with an Overhauser Proton Precession Marine Magnetometer, with a maximum resolution of 0.001 nT and a sample rate of 1 Hz, towed from the back deck of the vessel with a 280 m-long cable to a depth of 2 m below sea level. Magnetic profiles were acquired discontinuously along BOOST seismic lines 3 and 1. Magnetic anomaly data were corrected (i.e. IGRF 2020<sup>65</sup>) and processed with low-pass filtered (30 min).

During BGR-expedition GANOVEX IX airborne magnetic data were acquired by using a Twin Otter aircraft. The area was surveyed from a base camp on Edisto Glacier, with a line spacing of 5 km and tie line spacing of 25 km with a Scintrex CS-3 cesium magnetometer sensor and the survey was mainly conducted at a constant altitude of 600 m above sea level. The magnetic data was corrected and processed using Geosoft's Oasis Montaj geophysical software (e.g. de-spiking, core field correction, diurnal variations and levelling procedures). The analytical signal and maximum horizontal gradient are calculated and can be useful in the location of the edges of magnetic source bodies.

## Data availability

The data used to support the findings of this study are available from the corresponding author upon request.

Received: 15 January 2025; Accepted: 10 June 2025

## References

- Jordan, T. A., Riley, T. R. & Siddoway, C. S. The geological history and evolution of West Antarctica. *Nat. Rev. Earth Environ.* **1**, 117–133. <https://doi.org/10.1038/s43017-019-0013-6> (2020).
- Harry, D. L., Jourdan, L. A. & Sumant, J. Geodynamic models of the West Antarctic rift system: implications for the mantle thermal state. *Geosphere* **14**, 2407–2429. <https://doi.org/10.1130/GES01594.1>
- Salvini, F. et al. Cenozoic geodynamics of the Ross sea region, antarctica: crustal extension, intraplate strikeslip faulting and tectonic inheritance. *J. Geophys. Res.* **102**, 24669–24696 (1997).
- Cande, S. C., Stock, J. M., Muller, R. D. & Ishihara, T. Cenozoic motion between East and West Antarctica. *Nature* **404**, 145–150 (2000).
- Siddoway, C. S. Tectonics of the West Antarctic Rift System: New light on the history and dynamics of distributed intracontinental extension. In: *Antarctica: A Keystone in a Changing World. Proceedings of the 10th International Symposium on Antarctic Earth Sciences* (eds. Cooper, A. K., Barrett, P. J., Stagg, H., Storey, E., Wise, W.) 91–114 (The National Academies Press, 2008). <https://doi.org/10.3133/ofr20071047KP09>
- Granot, R., Cande, S. C., Stock, J. M., Davey, F. J. & Clayton, R. W. Postspreading rifting in the Adare basin, antarctica: regional tectonic consequences. *Geochem. Geophys. Geosys.* **11**, Q08005 (2010).
- Panter, K. S. et al. Melt origin across a rifted continental margin: a case for subduction-related metasomatic agents in the lithospheric source of alkaline basalt, NW Ross sea, Antarctica. *J. Petrol.* **59**, 517–558. <https://doi.org/10.1093/petrology/egy036> (2018).
- Durkin, K., Day, J. M. D., Panter, K. S., Xu, J. F. & Castillo, P. R. Petrogenesis of alkaline magmas across a continent to ocean transect, Northern Ross sea, Antarctica. *Chem. Geol.* **641**, 121780. <https://doi.org/10.1016/j.chemgeo.2023.121780> (2023).
- Smellie, J. L. & Rocchi, S. Chapter 5.1a Northern Victoria Land: volcanology. In *Volcanism in Antarctica: 200 Million Years of Subduction, Rifting and Continental Break-up* (eds. Smellie, J. L., Panter, K. S. & Geyer A.) 347–381 (Geol. Soc., 2021). <https://doi.org/10.1144/M55-2018-60>
- Hill, P. J. & Exon, N. F. Tectonics and basin development of the offshore Tasmanian area; incorporating results from deep ocean drilling. In: *The Cenozoic Southern Ocean: Tectonics, Sedimentation and Climate between Australia and Antarctica* (eds. Exon, N. F., Kennett, J. P., Malone, M.) *Geophys. Monogr. Ser.* 151, 19–42, AGU, Washington, D.C. (2004).
- Stickley, C. E. et al. Timing and nature of the deepening of the Tasmanian gateway. *Paleoceanography Paleoclimatology.* **19**, PA4027. <https://doi.org/10.1029/2004PA001022> (2004).
- Hodel, F. et al. Drake passage gateway opening and Antarctic circumpolar current onset 31 ma ago: the message of the neodymium isotope record. *Chem. Geol.* **570**, 120171. <https://doi.org/10.1016/j.chemgeo.2021.120171> (2021).
- Sijp, W. P. & England, M. H. Effect of the Drake passage throughflow on global climate. *J. Phys. Oceanogr.* **34**, 1254–1266 (2004).
- Klages, J. P. et al. Ice sheet-free West Antarctica during peak early oligocene glaciation. *Science* **385**, 322–327. <https://doi.org/10.1126/science.adj3931>
- Cande, S. C. & Stock, J. M. Pacific-Antarctic-Australia motion and the formation of the Macquarie plate. *Geophys. J. Int.* **157**, 399–414. <https://doi.org/10.1111/j.1365-246X.2004.02224.x> (2004).
- Granot, R. & Dymant, J. Late cenozoic unification of East and West Antarctica. *Nat. Commun.* **9**, 3189. <https://doi.org/10.1038/s41467-018-05270-w> (2018).
- Rossetti, F., Storti, F. & Läufer, A. Brittle architecture of the Lanterman fault and its impact on the final terrane assembly in North Victoria land, Antarctica. *J. Geol. Soc. Lond.* **159**, 159–173 (2002).
- Rossetti, F. et al. Eocene initiation of Ross sea dextral faulting and implications for East Antarctic neotectonics. *J. Geol. Soc. Lond.* **163**, 119–126 (2006).
- Kleinschmidt, G. & Läufer, A. The Matusевич fracture zone in oates land, East Antarctica. In: *Antarctica: Contributions To Global Earth Sciences* (eds Futterer, D. K., Damaske, D., Kleinschmidt, G., Miller, H. & Tessensohn, F.) Springer, Berlin, 175–180 (2006).
- Läufer, A., Damaske, D. & Lisker, F. Neogene tectonics in the Edisto and Tucker Inlet region and its correlation with offshore magnetic anomalies North of cape adare, Northern Victoria land, Antarctica. *Polarforschung* **80**, 111–126 (2011).
- Cianfarra, P. et al. Multiple reactivations of the Rennick Graben Fault system (northern Victoria Land, Antarctica): New evidence from paleostress analysis. *Tectonics* **41**, e2021TC007124 (2022). <https://doi.org/10.1029/2021TC007124>
- Ryan, W. B. F. et al. Global multi-resolution topography (GMRT) synthesis data set. *Geochem. Geophys. Geosyst.* **10**, Q03014. <https://doi.org/10.1029/2008GC002332> (2009).
- Vignaroli, G., Balsamo, F., Giordano, G., Rossetti, F. & Storti, F. Miocene-to-Quaternary oblique rifting signature in the Western Ross sea from fault patterns in the McMurdo volcanic group, North Victoria land, Antarctica. *Tectonophysics* **656**, 74–90 (2015).
- Dorschel, B. et al. The international bathymetric chart of the Southern ocean version 2 (IBCSO v2). *Sci. Data.* **9**, 275. <https://doi.org/10.1038/s41597-022-01366-7> (2022).
- Wellner, J. S., Heroy, D. C. & Anderson, J. B. The death mask of the Antarctic ice sheet: comparison of glacial geomorphic features across the continental shelf. *Geomorphology* **75**, 157–171. <https://doi.org/10.1016/j.geomorph.2005.05.015> (2006).
- King, E. C., Hindmarsh, R. C. A. & Stokes, C. R. Formation of mega-scale glacial lineations observed beneath a West Antarctic ice stream. *Nat. Geosci.* **2**, 585–588 (2009).

27. Stokes, C. R. et al. Formation of mega-scale glacial lineations on the Dubawnt lake ice stream bed: 1. Size, shape and spacing from a large remote sensing dataset. *Q. Sci. Rev.* **77**, 190–209. <https://doi.org/10.1016/j.quascirev.2013.06.003> (2013).
28. King, E. L., Sejrup, H. P., Haflidason, H., Elverhøi, A. & Aarseth, I. Quaternary seismic stratigraphy of the North sea fan: glacially-fed gravity flow aprons, hemipelagic sediments, and large submarine slides. *Mar. Geol.* **130**, 293–315 (1996).
29. Dowdeswell, J. A. et al. A major trough-mouth fan on the continental margin of the Bellingshausen sea, West antarctica: the belgica fan. *Mar. Geol.* **252**, 129–140. <https://doi.org/10.1016/j.margeo.2008.03.017> (2008).
30. Rebesco, M., Hernández-Molina, F. J., Van Rooij, D. & Wählin, A. Contourites and associated sediments controlled by deep-water circulation processes: State-of-the-art and future considerations. *Mar. Geol.* **352**, 111–154. <https://doi.org/10.1016/j.margeo.2014.03.011> (2014).
31. Hayes, D. E. & Frakes, L. A. General synthesis, Deep Sea drilling Project Leg 28. In *Initial reports of the Deep Sea drilling Project* (ed. Kaneps, A. G.). 28 (U.S. Government Printing Office, 1975).
32. Jovane, L. et al. Magnetostratigraphic chronology of a cenozoic sequence from DSDP site 274, Ross sea, Antarctica. *Front. Earth Sci.* **8**, 563453. <https://doi.org/10.3389/feart.2020.563453> (2020).
33. Brancolini, G. et al. ANTOSTRAT Project, seismic stratigraphic atlas of the Ross Sea, Antarctica. In: *Geology and Seismic Stratigraphy of the Antarctic Margin* (eds. Cooper, A.K., Barker, P.F., Brancolini, G.). Antarct. Res. Ser. (Washington, D.C.) 68, AGU (1995).
34. Davey, F. J., Brancolini, G., Hamilton, R. J., Henrys, S. & Sorlien, C. C. A revised correlation of the seismic stratigraphy at the cape Roberts drill sites with the seismic stratigraphy of the Victoria land basin, Antarctica. *Terra Antarctica.* **7** (3), 215–220 (2000).
35. Sauli, C. et al. Neogene development of the terror rift, Western Ross sea, Antarctica. *Geochem. Geophys. Geosyst.* **22**, e2020GC009076. <https://doi.org/10.1029/2020GC009076> (2021).
36. Hinz, K. & Block, M. Results of geophysical investigations in the Weddell Sea and in the Ross Sea, Antarctica. In: *Proceedings of the 11th World Petroleum Congress: Chichester, London, UK, John Wiley & Sons, Geology Exploration Reserves 2*, 79–91 (1984).
37. Busetti, M., De Santis, L., Kavun, M. & Zayatz, I. Seismic sequences of the Ross sea continental margin (Antarctica). *Boll. Geofis. Teor. App.* **35**, 133–152 (1993).
38. (eds Cooper, A. K., Barker, P. F. & Brancolini, G.). *Geology and Seismic Stratigraphy of the Antarctic Margin* Washington, D. C. American Geophysical Union 303 (Antarctic Research Series, 68) (1995). <https://doi.org/10.1029/ar068>
39. Soares, D. M., Alves, T. M. & Terrinha, P. The breakup sequence and associated lithospheric breakup surface: their significance in the context of rifted continental margins (West Iberia and Newfoundland margins, North Atlantic). *Earth Planet. Sci. Lett.* **355–356**, 311–326. <https://doi.org/10.1016/j.epsl.2012.08.036> (2012).
40. Alves, T. et al. A tectono-stratigraphic review of continental breakup on intraplate continental margins and its impact on resultant hydrocarbon systems. *Mar. Pet. Geol.* **117**, 104341. <https://doi.org/10.1016/j.marpetgeo.2020.104341> (2020).
41. Goldner, A., Herold, N. & Huber, M. Antarctic glaciation caused ocean circulation changes at the Eocene-Oligocene transition. *Nature* **511**, 574–577. <https://doi.org/10.1038/nature13597> (2014).
42. Sangiorgi, F. et al. Southern ocean warming and Wilkes land ice sheet retreat during the mid-Miocene. *Nat. Commun.* **9** (1), 317 (2018).
43. Pérez, L. F. et al. Miocene ice sheet dynamics in the Westernmost Ross sea (Antarctica): regional correlations. *Global Planet. Change.* **216**, 10391. <https://doi.org/10.1016/j.gloplacha.2022.103891> (2022).
44. Pérez, L. F. et al. IODP expedition 374 scientists. Early and middle miocene ice sheet dynamics in the Ross sea: results from integrated core-log-seismic interpretation. *GSA Bull.* **134**, 348–370. <https://doi.org/10.1130/B35814.1> (2021).
45. Naish, T. et al. Obliquity-paced pliocene West Antarctic ice sheet oscillations. *Nature* **458**, 322–328. <https://doi.org/10.1038/nature07867> (2009).
46. Dolan, A. M., De Boer, B., Bernales, J., Hill, D. J. & Haywood, A. M. High climate model dependency of pliocene Antarctic ice-sheet predictions. *Nat. Commun.* **9**, 2799. <https://doi.org/10.1038/s41467-018-05179-4> (2018).
47. Mas et al. A thicker Antarctic ice stream during the mid-Pliocene warm period. *Commun. Earth Environ.* **4**, 321. <https://doi.org/10.1038/s43247-023-00983-3> (2023).
48. Savage, M. L. & Ciesielski, P. F. A revised history of glacial sedimentation in the Ross Sea region. In: *Antarctic Earth Science. Proceedings of the Fourth International Symposium on Antarctic Earth Science* (eds. Oliver, R. L., James, P. R. & Jago J. B.) 555–559, Australian Academy of Science, Canberra, Australia (1983).
49. Jamtveit, B., Svensen, H., Podladchikov, Y. Y. & Planke, S. Hydrothermal vent complexes associated with sill intrusions in sedimentary basins. In: *Physical Geology of High-Level Magmatic Systems* (eds. Breitreuz, C. & Petford, N.). *Geol. Soc. London Spec. Publ.* **234**, 233–241 (2004).
50. Planke, S., Rasmussen, T., Rey, S. S. & Myklebust, R. Seismic characteristics and distribution of volcanic intrusions and hydrothermal vent complexes in the Vøring and Møre basins. In: *Petroleum Geology: North-West Europe and Global Perspectives* (eds. Doré, A. G. & Vining, B. A.). Proceedings of the 6th Petroleum Geology Conference, 833–844. Petroleum Geology Conferences Ltd. Published by the Geological Society, London (2005).
51. Olakunle, O. K., Ajibola, L. M., Muhammad, I. H. & Makovsky, Y. Massive seafloor mounds depict potential for seafloor mineral deposits in the great South basin (GSB) offshore new Zealand. *Sci. Rep.* **11**, 9185. <https://doi.org/10.1038/s41598-021-88620-x> (2021).
52. Galland, O. et al. Storage and transport of magma in the layered crust-formation of sills and related flat-lying intrusions. In *Volcanic and Igneous Plumbing Systems: Understanding Magma Transport, Storage, and Evolution in the Earth's Crust* (ed. Burchardt, S.) 113–138 (Elsevier, 2018).
53. Damaske, D. et al. Magnetic anomalies north-east of Cape Adare, northern Victoria Land (Antarctica), and their relation to onshore structures. In: *Antarctica: A Keystone in a Changing World* (eds. Cooper, A. K., Raymond, C. R. Online Proceedings of the 10th ISAES, USGS Open-File Report 2007 – 1047, Short Res. Paper 016 (2007). <https://doi.org/10.3133/of2007-1047.srp016>
54. Golynsky, A. V. et al. ADMAP2 Magnetic anomaly map of the Antarctic - links to ADMAP2 gdb files [dataset]. PANGAEA, (2018). <https://doi.org/10.1594/PANGAEA.892721>. In supplement to: Golynsky, A. V. : New magnetic anomaly map of the Antarctic. *Geophysical Research Letters* **45**(13), 6437–6449 (2018). <https://doi.org/10.1029/2018GL078153>.
55. Cox, S. C. et al. The geomap (v.2022-08) continent-wide detailed geological dataset of Antarctica [dataset]. PANGAEA <https://doi.org/10.1594/PANGAEA.951482> (2023).
56. Läufer, A., Lisker, F. & Phillips, G. Late Ross-orogenic deformation of basement rocks in the Northern deep freeze range, Victoria land, antarctica: the lichen hills shear zone. *Polarforschung, bremerhaven, Alfred wegener Institute for Polar and marine research. German Soc. Polar Res.* **80**(2), 60–70 (2011).
57. Rossetti, F., Storti, F. & Salvini, F. Cenozoic noncoaxial transtension along the Western shoulder of the Ross sea, antarctica, and the emplacement of McMurdo Dyke arrays. *Terra Nova.* **12**(2), 60–66. <https://doi.org/10.1111/j.1365-3121.2000.00270.x> (2000).
58. Lloyd, A. J. et al. Seismic structure of the Antarctic upper mantle imaged with adjoint tomography. *JGR Solid Earth.* **124** <https://doi.org/10.1029/2019JB017823> (2019).
59. Chua, E. L. & Lebedev, S. Waveform tomography of the Antarctic plate. *Geophys. J. Int.* **241** (1), 219–240. <https://doi.org/10.1093/gji/ggaf041> (2025).
60. Cande, S. C. & Stock, J. M. Cenozoic reconstructions of the Australia-New Zealand-South Pacific sector of Antarctica. In: *The Cenozoic Southern Ocean: Tectonics, Sedimentation and Climate Change Between Australia and Antarctica* (eds Exon, N. F., Kennett J. K., & Malone M. J.). *Geophys. Monogr. Ser.* **148**, 5–18 (AGU, 2004). <https://doi.org/10.1029/151GM02>

61. DeMets, C., Gordon, R. G. & Argus, D. F. Geologically current plate motions. *Geophys. J. Int.* **181**, 1–80. <https://doi.org/10.1111/j.1365-246X.2009.04491.x> (2010).
62. Gibson, G. et al. Pre-existing basement structure and its influence on continental rifting and fracture zone development along australia's Southern rifted margin. *J. Geol. Soc.* **170**, 365–377. <https://doi.org/10.1144/jgs2012-040> (2013).
63. Exon, N. F., Kennett, J. P. & Malone, M. J. Leg 189 synthesis: Cretaceous–Holocene history of the Tasmanian Gateway. In: *Proc. ODP, Sci. Results* 189 (eds. Exon, N. F., Kennett, J. P. & Malone, M. J.), (Ocean Drilling Program, 2004).
64. Storti, F., Salvini, F. & Rossetti, F. Phipps morgan, J. Intraplate termination of transform faulting within the Antarctic continent. *Earth Planet. Sci. Lett.* **260**, 115–126 (2007).
65. Alken, P. et al. International geomagnetic reference field: thirteenth generation. *Earth Planet Space.* **73**, 49. <https://doi.org/10.1186/s40623-020-01288-x> (2021).

## Acknowledgements

This study was carried out in the framework of the BOOST International Project (Bridging Onshore-Offshore Structures at the Pacific Coast of North Victoria Land, Antarctica: an integrated approach), a research project funded by PNRA (Programma Nazionale di Ricerca in Antartide) and by BGR (Federal Institute for Geosciences and Natural Resources). We thank C. Frassi, and 3 anonymous reviewers for their insightful comments and constructive suggestions that improved our manuscript. We wish to express our gratitude to the crew and the scientific and technical party on board the OGS R/V Laura Bassi for their support in data acquisition at sea during the 38th and 39th Italian Antarctic Expeditions (February 2023 and 2024). We would also like to acknowledge the GANOVEX IX team for aeromagnetic data acquisition.

## Author contributions

D.C. and L.C. contributed equally to the present study (first authors) by conceptualizing the work, analyzing and interpreting the seismic data and the multibeam morpho-bathymetric data, writing the first draft of the manuscript and preparing the figures, A.R. processed and interpreted the aeromagnetic data, wrote the first draft of the manuscript and prepared the figures, G.M.F. data acquisition, processing of the seismic and magnetic data, D.M. data acquisition, contribution to data interpretation, D.A. data acquisition and processing of the multibeam morpho-bathymetric data, F.A. contributed to the processing of the seismic data and their interpretation, M.L. data acquisition, contribution to data interpretation, V.V., M.B. and E.A. contributed to the data interpretation. A.L. conceptualized the work, interpreted the data and wrote the first draft of the manuscript; all authors discussed and commented on the methods and results and contributed to the final version of the paper.

## Funding

Funding for this research was provided by PNRA19\_00051-A1\_BOOST (Programma Nazionale di Ricerca in Antartide) and the Federal Institute for Geosciences and Natural Resources (BGR).

## Declarations

### Competing interests

The authors declare no competing interests.

## Additional information

**Supplementary Information** The online version contains supplementary material available at <https://doi.org/10.1038/s41598-025-06739-7>.

**Correspondence** and requests for materials should be addressed to D.C.

**Reprints and permissions information** is available at [www.nature.com/reprints](http://www.nature.com/reprints).

**Publisher's note** Springer Nature remains neutral with regard to jurisdictional claims in published maps and institutional affiliations.

**Open Access** This article is licensed under a Creative Commons Attribution-NonCommercial-NoDerivatives 4.0 International License, which permits any non-commercial use, sharing, distribution and reproduction in any medium or format, as long as you give appropriate credit to the original author(s) and the source, provide a link to the Creative Commons licence, and indicate if you modified the licensed material. You do not have permission under this licence to share adapted material derived from this article or parts of it. The images or other third party material in this article are included in the article's Creative Commons licence, unless indicated otherwise in a credit line to the material. If material is not included in the article's Creative Commons licence and your intended use is not permitted by statutory regulation or exceeds the permitted use, you will need to obtain permission directly from the copyright holder. To view a copy of this licence, visit <http://creativecommons.org/licenses/by-nc-nd/4.0/>.

© The Author(s) 2025

# INVOICE

Springer Nature Customer Service Center GmbH [www.springernature.com](http://www.springernature.com)  
 Europaplatz 3  
 69115 Heidelberg | Germany  
 VAT ID.DE209719094

## SPRINGER NATURE GROUP

<b>Our Reference No.</b> > 2936498027	<b>Finance Account No.</b> > 2202973030	<b>Customer Account No.</b> > 3007660748	<b>Purchase Order No.</b> >	<b>Customer VAT ID</b> > IT00055590327	<b>Date</b> 16.06.2025	<b>Pages</b> 1 / 2
--	--	---	--------------------------------	---	---------------------------	-----------------------

Bill to	Ship to
> OGS Borgo Grotta Gigante 42/C 34010 Sgonico ( TS ) Italy	Dario Civile OGS Borgo Grotta Gigante 42/C 34010 Sgonico ( TS ) Italy

Quantity	Product No.	Description	List Price	Disc. %	VAT	Amount
1	43930E	Single APC Order: 0019485177 Open: Man Apc price Open: man.ReducePr. Open:APC+ Discount  Manuscript ID: 8CE68325-CF2F-4F68-A8FC-F4085BB4E6B DOI:10.1038/S41598-025-06739-7 Journal Name: Scientific Reports Author Name: Dario Civile Manuscript Title:Discovery of cenozoic magmatic ridges and tectonics off Northern Victoria land provides new insights into the geody Customer to self-assess VAT (reverse charge), Article 44 & 196 of EC Directive 2006/112	2.390,00 2.390,00		A	2.390,00
1	80078E	Single APC Admin Fee Order: 0019485177 Open: Admin Fee Customer to self-assess VAT (reverse charge), Article 44 & 196 of EC Directive 2006/112	55,00		A	55,00
		VAT Reverse Charge, the customer is liable for the VAT due <b>The European Union's (EU) General Product Safety Regulation (GPSR) is a set of rules that requires consumer products to be safe and our obligations to ensure this.</b>  <b>If you have any concerns about our products, you can contact us at: <a href="mailto:ProductSafety@springernature.com">ProductSafety@springernature.com</a></b>  <b>In case Publisher is established outside the EU, the EU authorized representative is:</b> <b>Springer Nature Customer Service Center GmbH</b> <b>Europaplatz 3</b> <b>69115 Heidelberg, Germany</b>				

<b>Subtotal</b>						2.445,00
-----------------	--	--	--	--	--	----------

# INVOICE

Springer Nature Customer Service Center GmbH [www.springernature.com](http://www.springernature.com)  
 Europaplatz 3  
 69115 Heidelberg | Germany  
 VAT ID.DE209719094

## SPRINGER NATURE GROUP

<b>Our Reference No.</b> > 2936498027	<b>Finance Account No.</b> > 2202973030	<b>Customer Account No.</b> > 3007660748	<b>Purchase Order No.</b> >	<b>Customer VAT ID</b> > IT00055590327	<b>Date</b> 16.06.2025	<b>Pages</b> 2 / 2
--	--	---	--------------------------------	---	---------------------------	-----------------------

--	--	--	--	--	--	--

<b>Net Value Goods C</b>	0,00	<b>Net Value Goods B</b>	0,00	<b>Net Value Goods A</b>	2.445,00	<b>Total Net Value of Goods</b>	2.445,00
<b>Net Shipping Costs C</b>	0,00	<b>Net Shipping Costs B</b>	0,00	<b>Net Shipping Costs A</b>	0,00	<b>Total Net Shipping Costs</b>	0,00
<b>Total Net C</b>	0,00	<b>Total Net B</b>	0,00	<b>Total Net A</b>	2.445,00	<b>Total Net Due</b>	2.445,00
<b>Incoterms DDP</b>	<b>VAT C</b>	<b>VAT B</b>	<b>VAT A</b>	<b>Total VAT</b>		0,00	
<b>Subtotal</b>							2.445,00
<b>Prepaid</b>							0,00
<b>TOTAL DUE</b>						<b>EUR</b>	<b>2.445,00</b>

**Questions regarding this order?**

> Fon: +44(0) 293 192 2009  
 For queries or assistance, please contact **ORSsupport@springernature.com**  
 For Remittance Advice and proof of payment, please email them at **ARadvice@springernature.com**  
 For overdue and pre collection letters: **Collections.OpenAccess@springernature.com**  
 For supplier Portal and invoice upload contact **orsupportadmin@springernature.com**

Remit a payment in Euro to:  
 Bank details: **Hypovereinsbank München**  
 Account: 654793298 - Sort code : 70020270  
 IBAN: DE22 7002 0270 0654 7932 98  
 BIC: HYVEDEMMXXX

To pay by credit card:  
 Scan QR-code or send an E-mail to: **creditcardstm@springernature.com**  
 for a secure payment link  
 Do not send us your credit card details



**Payable net 30 days**

**Thank you for your order.**

